Nested Space Mapping Technique for Design and Optimization of Complex Microwave Structures with Enhanced Functionality

Slawomir Koziel, Adrian Bekasiewicz, and Piotr Kurgan

Abstract In this work, we discuss a robust simulation-driven methodology for rapid and reliable design of complex microwave/RF circuits with enhanced functionality. Our approach exploits nested space mapping (NSM) technology, which is dedicated to expedite simulation-driven design optimization of computationally demanding microwave structures with complex topologies. The enhanced functionality of the developed circuits is achieved by means of slow-wave resonant structures (SWRSs), used as replacement components for conventional transmission lines. The NSM is a hierarchical, bottom-up methodology, in which the inner space mapping layer is applied to improve generalization capabilities of the equivalent circuit constructed on the SWRS level, whereas the outer layer is used to enhance the surrogate model of the entire structure of interest. We demonstrate that the NSM significantly improves the performance of traditional surrogate-based optimization routines applied to the design problem of computationally expensive microwave/RF structures with modular topology. The proposed technique is used to design three exemplary microwave/RF circuits with enhanced functionality: two abbreviated microstrip matching transformers and a miniaturized rat-race coupler with harmonic suppression. We also provide a comprehensive comparison with other surrogate-assisted methods, as well as supply the reader with basic design guidelines for the state-of-the-art SWRS-based microwave/RF circuits.

Keywords Microwave/RF circuit • Surrogate model • Electromagnetic (EM) simulation • Nested space mapping • Surrogate-based optimization • Slow-wave resonant structure (SWRS) • Uniform transmission line • Two-level modeling • Microstrip circuit

S. Koziel (✉)
Engineering Optimization & Modeling Center, School of Science and Engineering,
Reykjavik University, Menntavegur 1, 101 Reykjavik, Iceland
e-mail: koziel@ru.is

A. Bekasiewicz (✉) • P. Kurgan
Faculty of Electronics, Telecommunications and Informatics, Gdansk University of Technology,
Narutowicza 11/12, 80-233 Gdansk, Poland
e-mail: adrian.bekasiewicz@pg.gda.pl

© Springer International Publishing Switzerland 2014

S. Koziel et al. (eds.), *Solving Computationally Expensive Engineering Problems*,
Springer Proceedings in Mathematics & Statistics 97,
DOI 10.1007/978-3-319-08985-0_3

1 Introduction

Modern wireless communication systems impose stringent requirements upon microwave and radio-frequency (RF) blocks, placing particular emphasis on passive components. These commonly used circuits are required to satisfy strictly defined system specifications, e.g., multiband [1–3], or wideband operation [4–6], attenuation of harmonic frequencies [7–9], high isolation [10–12], etc. Moreover, physical dimensions of passive components are also regulated by available, often limited estate area [13–15]. In general, traditional theory-based design routines are incapable of providing reliable design solutions when circuit size and its performance are simultaneously taken into consideration [16, 17]. Among variety of techniques dedicated to enhance the functionality of conventional passive components [18–22], the modification of circuit's geometry by means of intentional perturbations, defects, or discontinuities—implemented in either metallization plane—has gained increased attention as the most promising method to perform a cost-efficient microwave/RF circuit refinement [23–25].

Although the implementation of various perturbations and discontinuities may be extremely beneficial from the perspective of the functionality of microwave/RF structures—both geometrical- and performance-wise—it simultaneously hinders the design process due to the increased number of designable parameters that have to be simultaneously adjusted to yield a proper operation of the circuit [26, 27]. A typical experience-based design approach using repetitive parameter sweeps is suitable for tuning only one parameter at a time and, therefore, its utilization is limited for multi-dimensional design spaces of microwave/RF circuits with complex topologies. Consequently, the design of microwave/RF structures with enhanced functionality is considered to be a multifaceted problem that may be addressed only by means of numerical optimization.

Reliable design optimization of highly miniaturized microwave/RF components is an extremely challenging issue of contemporary wireless communication engineering. The main reason for it is the lack of computationally cheap and accurate theoretical models representing the behavior of such unconventional structures. Unfortunately, a reliable performance evaluation of complex microwave/RF components, and—consequently—their design, can only be achieved through CPU-intensive electromagnetic (EM) simulations. As opposed to conventional microwave/RF circuits, EM models of sophisticated structures with enhanced functionality are, in general, computationally expensive, which is another crucial factor hindering the design process. Additionally, a large number of independent designable parameters involved in structure optimization significantly increases numerical complexity of the process, as well as the number of EM evaluations necessary to complete the optimization task. Hence, direct EM-based optimization using conventional gradient [28] or derivative-free [29] algorithms is normally prohibitive. On the other hand, techniques such as adjoint sensitivity [30, 31] allow for low-cost derivative evaluation, which may lead to substantial cost reduction of gradient-based search procedures [32, 33]. However, this technology is not yet

widely available in commercial computer-aided design (CAD) software. Another important issue related to conventional optimization techniques is their local convergence properties, i.e., the ability to find only a local optimum (usually the one closest to the initial design). The aforementioned difficulty may be partially addressed by global optimization methods. In practice, this means resorting to population-based metaheuristics, which are even more expensive—computational-wise—than local-search algorithms [34, 35]. For that reason, the utilization of direct optimization techniques in the design and optimization of complex circuits is usually impractical.

High-computational cost related to the design of compact microwave/RF structures may be partially alleviated by means of surrogate-based optimization (SBO) techniques [36], including, among others, manifold mapping [37, 38], shape preserving response prediction [39, 40], or space mapping [41, 42]. The attractiveness of the SBO lies in its ability to iteratively correct/enhance a low-fidelity model using a limited amount of data acquired from simulations of a high-fidelity model [43]. SBO methods gained a considerable attention in diverse engineering fields [44–46] and proved to be very efficient design methodologies, capable of yielding desired solutions at the cost of only a few simulations of respective high-fidelity models. Space mapping—originated in the field of microwave technology—is particularly interesting in the context of numerically complex circuit design, especially due to its simple implementation [47, 48], high efficiency [43, 49], and successful validation on a variety of microwave structures [27, 43, 49]. On the other hand, SBO techniques, especially space mapping algorithms, are mostly used for the expedited design and optimization of conventional microwave/RF circuits [47, 49]. Although several methods regarding this concept have been proposed for optimization of complex structures [27, 50] they require inconvenient manual setup of multiple optimization problems and are problematic when large number of parameters is involved [51].

In this chapter, we provide general guidelines for the development of unconventional microwave/RF circuits with enhanced functionality. This is achieved through the decomposition of a conventional circuit into its elementary building blocks, more particularly uniform transmission lines (TLs) and their subsequent replacement with unconventional (e.g., shortened, dual-band, etc.) slow-wave structures. Moreover, challenges and benefits regarding the design of SWRS-based circuit are presented. Next, we introduce a nested space mapping (NSM) technology aimed at fast and accurate design of computationally expensive planar microwave/RF components. NSM constructs a two-stage low-fidelity model, with the inner space mapping layer applied at the level of the decomposed TL, and the outer space mapping layer applied for the entire circuit. The proposed technique mitigates the problem of surrogate model inaccuracy resulting from complex layouts of unconventional circuits and enables its rapid optimization in a single run of the algorithm.

The chapter is organized as follows. In Sect. 2, we discuss the concept of circuit functionality enhancements based on its decomposition and a subsequent refinement of its elementary building blocks using SWRSs. We also explain techniques for

the construction of SWRSs and their influence on the behavior of the entire microwave/RF circuit. Sect. 3 is devoted to the problem of complex microwave circuits design using surrogate-based optimization. We briefly formulate a SBO design task and introduce the concept of NSM, numerical methods used to construct an accurate surrogate model, as well as generalization capabilities of the developed surrogate models. Verification of the introduced methodology on the basis of several illustrative examples is given is Sect. 4. Two shortened matching transformers and a miniaturized rat-race coupler with harmonic suppression are considered for the design and optimization using the NSM. Section 5 concludes the chapter with a discussion and recommendations for the future research related to fast design and optimization of complex structures with enhanced functionality.

2 Design of Complex Microwave Circuits: Methodology

Design of complex microwave/RF circuits with enhanced functionality is troublesome, especially due to the lack of universal strategies for determination of their topology. In general, three approaches for the design of unconventional circuits are available, including: (1) manual, experience-based construction [52, 53] (2) structure decomposition and substitution of its sections with unconventional structures [54, 55], and (3) automated design by means of metaheuristic algorithms [56, 57].

While the first technique benefits from many degrees of freedom that allow for the construction of novel structures with unusual properties (both geometry- and performance-wise), possible results strongly depend on engineering experience. In such a setup, the design process is conducted using cut and trial technique, often in conjunction with repetitive parameter sweeps. Therefore, the method is laborious and prone to failure, which restricts its applicability to designs with relatively simple topologies with up to several independent parameters [58, 59].

Improved properties of the circuit may also be obtained through decomposition of a conventional structure into a set of TL sections. Each TL may be subsequently replaced with its discontinuous counterpart and modified sections may be utilized for the construction of an unconventional structure. Despite the manual setup of the aforementioned steps, the risk of design failure in such a scheme is alleviated by using discontinuous TL components with simplified geometry that mimic the behavior of their conventional TLs. Furthermore, a lot of perforations from the literature may be directly utilized to substitute typical TL sections [60–63], which makes the technique useful, even for less experienced engineers. One should note that the method is restricted only to certain microwave/RF structures that may be decomposed, however a variety of passive circuits fall into this category, e.g., matching transformers, hybrid couplers, Butler matrices, phase shifters, or planar filters.

Although methods based on the manual design of circuits with unconventional properties are most commonly used, some automated approaches for a construction

of such structures are also available [56, 64–66]. Automated design is especially attractive for inexperienced engineers as it reduces the interference into the design process only to formulating the desired performance specifications. Design of a microwave/RF structure in such a setup may be conducted using either EM model generated from binary matrix [56, 64] or interconnected TL sections [65, 66]. While the former technique allows for a construction of very compact circuits, it requires a number of computationally expensive EM simulations for a metaheuristic algorithm to complete. The latter method is considerably faster because it exploits circuit simulator instead of EM one. On the other hand, it suffers from lack of support for the reduction of the overall circuit size.

In this section, we give general guidelines for the construction of microwave/RF circuits with enhanced functionality. Moreover, we instruct how to identify TL sections of a conventional circuit that may be extracted from the design. Two main approaches for the determination of sufficient perforations are discussed.

2.1 Construction of a Circuit with Enhanced Functionality

Modifications of a microwave/RF structure by a substitution of its TL sections with their corresponding perforations may be utilized to obtain some unconventional circuit behavior (e.g., attenuation of harmonic frequencies [50], high circuit selectivity [67], and/or broad operational band [68]) or advantageous physical dimensions [69]. One should bear in mind that techniques mentioned in this section require the preparation of a conventional circuit for its further modifications, however theory-based design of microstrip structures is well described in the literature (e.g., in [17, 70, 71]) and, for the sake of brevity, we omit details of their formulation.

The general flow (see Fig. 1 for a detailed block diagram with conceptual explanation of each step) of an unconventional structure design may be summarized as follows:

1. Define design specification of a circuit with enhanced functionality;
2. Synthesize conventional circuit using theory-based approach;
3. Decompose circuit into k sections that may be substituted with respective perforations;
4. Construct n abbreviated sections suitable for UTL replacement;
5. Perform surrogate-based design and optimization of the circuit.

In general, a conventional structure is composed of various building blocks, including: conventional lines (TL and/or coupled line sections) as well as their interconnections (e.g., bends, tees, crosses, etc.) [27]. This modular design allows to perform a so-called circuit decomposition step, which is a procedure—guided by engineering experience—aimed at identification of sections that may be important for functionality enhancements of the structure. While interconnections between consecutive sections are considered irrelevant, a total of k (where $k = 1, \ldots, K$) coupled lines and/or TLs may be distinguished and isolated from the circuit.

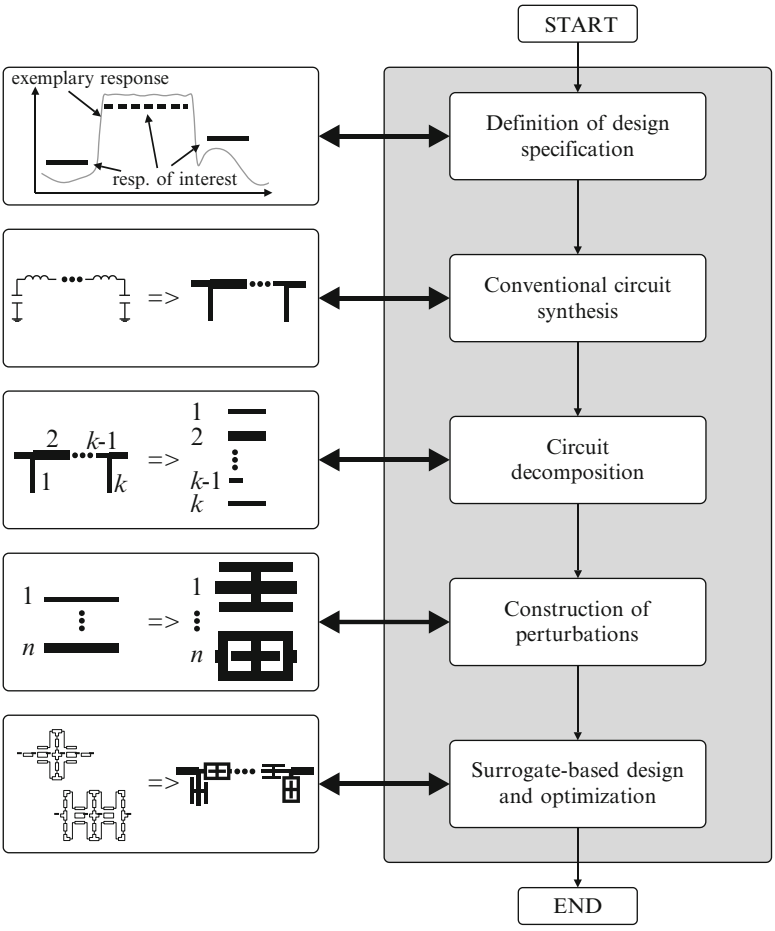

Fig. 1 Construction of a circuit with enhanced functionality by substituting conventional TL sections with perturbations—a design flow. In the first step, design specification is defined. Subsequently, general circuit line theory is utilized for a synthesis of a reference microstrip circuit. Next, the structure is decomposed into k conventional lines. In the fourth step, a set of n perturbations is designed in order to substitute their conventional counterparts. Finally, surrogate-based design driven by algorithm described in Sect. 3 is performed

Identification of respective sections is a crucial step for the determination of n (where $n = 1, \ldots, N$) different perturbations that are necessary to substitute their conventional counterparts. Exemplary microwave/RF circuits realized in microstrip technology with highlight of decomposition-ready sections are shown in Fig. 2.

A number of perturbations necessary to achieve desired functionality depend on such global factors such as desired bandwidth and/or geometry of the structure [69, 72], as well as local properties regarding characteristic impedance Z_C, electrical length θ (for TLs), and the coupling coefficient (for coupled lines). For that reason,

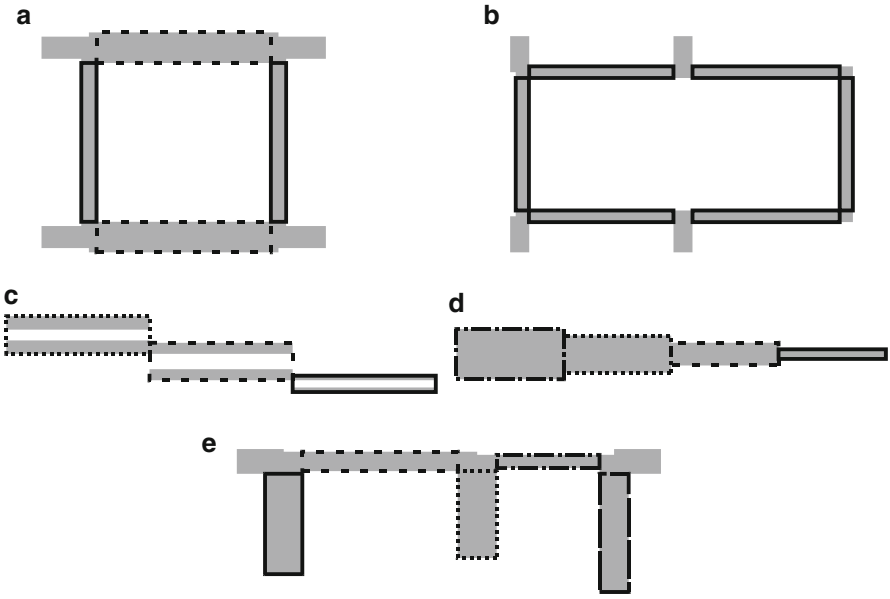

Fig. 2 Exemplary conventional microstrip circuits with highlighted relevant section: (**a**) brachline coupler —two TL sections with different characteristic impedance: (——) and (– – –); (**b**) rat-race coupler —one TL section: (——); (**c**) band-pass filter —three coupled line sections: (——), (– – –) and (•••); (**d**) impedance matching transformer —four TL section: (——), (——), (•••), (• – • –); (**e**) open-stub filter —five TL sections: (——), (– – –), (•••) (• – • –), (— —)

a number of necessary perturbations as well as their geometry should be carefully chosen for realization of specified design requirements. Although substantial research effort has been devoted towards the determination of perturbations with novel topologies over the years [60–63], only a few works attempted to address—in a systematic manner—the issue of their applicability for various unconventional designs [27, 50, 73]. However, in general, this problem may be solved only by means of engineering expertise, aided by some guidelines pointed out below:

- Substitution of conventional section with a cascade connection of perturbations allows for the bandwidth enhancement [24].
- Single perturbation is capable of realizing a range of Z_C and θ parameters and, therefore, it may substitute variety of corresponding TL sections [27].
- Miniaturization of asymmetric conventional circuit enforces preparation of a set of perturbations to mimic TL with equal electrical properties [69].

Several classes of perturbations, including: defected ground structures (DGS) [24], fractal space filing curves [67], or slow-wave resonant structures (SWRS) [50] may be exploited to mimic the behavior of conventional microwave/RF circuit components in a restricted frequency range. On the other hand, implementation of

perforations not only increases the complexity of the structure, but also introduces multiple independent design parameters that highly influence its performance. Design and optimization of such circuits is considered to be a computationally expensive problem that may be partially addressed using SBO algorithms [27]. Perturbations in the form of SWRS are particularly attractive for SBO setup because—in contrary to fractal curves and DGSs—they may be designed using a circuit simulator. Moreover, SWRS introduces slow-wave phenomenon that allows for decreasing the phase velocity, and consequently such perforations are shorter than conventional transmission lines. Nonetheless, a large number of variables associated with such circuits introduce serious problems with convergence of conventional SBO algorithms [51]. Techniques for the design of SWRS are described in Sects. 2.2 and 2.3, whereas SBO-based design and optimization of unconventional circuits with multiple perturbations are addressed in Sect. 3.

2.2 *Design of Slow-Wave Resonant Structures: Database Approach*

The choice of proper SWRS for a construction of a microwave/RF circuit with enhanced functionality is troublesome. The design of SWRS that may be considered to be a sufficient replacement of its corresponding UTL (or coupled line) is mostly conducted using cut and trial technique guided by engineering experience, which is a time consuming process involving numerous EM simulations. On the other hand, determination of appropriate SWRS may be conducted by gathering EM models of various predefined components. Such a database comprises an extensive description of each SWRS, including a number and range of design variables, as well as electric properties. Moreover, it provides tools for the identification of structures being most appropriate for realization of desired circuit behavior [73]. Several approaches that exploit database for the construction of unconventional circuits are available in literature [27, 50, 73]. Figure 3 depicts a set of exemplary SWRSs that may be utilized for the construction of a database.

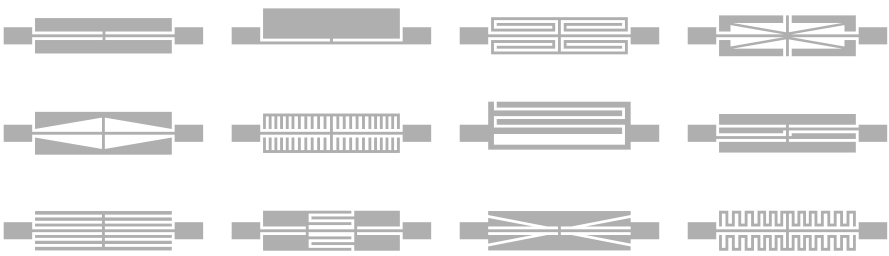

Fig. 3 An exemplary database containing 12 EM models of SWRSs [73]

The most appropriate SWRS is selected from the database by means of cell assessment with respect to defined efficiency coefficients, which may refer to local properties (e.g., range of Z_C and θ realizations, or transverse dimension of the SWRS) as well as global properties (e.g., bandwidth, or overall size) of the circuit (cf. Sect. 2.1). Each SWRS is evaluated with respect to all of its coefficients by computation of their weighted mean and a component with the best value is considered as sufficient to substitute respective conventional section. This technique may be also utilized for the selection of the most versatile SWRS to work as a substitute component of conventional sections with varied electrical parameters (c.f. Sect. 2.1). More detailed explanation of SWRS determination technique by means of a database utilization is presented in [73]. One should emphasize that a construction of a database comprising a number of EM models of SWRS requires considerable computational effort, however, once prepared, it may be reused multiple times with no extra computational cost.

2.3 *Design of Slow-Wave Resonant Structures: Knowledge-Based Approach*

Although design of unconventional circuit constituted by SWRS obtained from a predefined database is considerably easier in comparison to knowledge-based approach, it suffers from a smaller number of degrees of freedom in the process of forming a component into the desired shape. SWRSs gathered in database exhibit similarities that prevent their utilization for the design of structures with very unusual properties (e.g., very compact circuit [69], or wide range of electrical properties [27]). Therefore, SWRS designed exclusively for a specific circuit may provide the best results regarding desired specification. Additionally, a knowledge-based approach allows for a construction of complementary SWRSs (i.e., cells that geometrically supplement each other [69]), which is especially useful in the design of very compact circuits (e.g., [69, 73, 74]).

Despite the manual nature of the described SWRS design technique, some mathematical models aimed at the determination of its initial dimensions may be provided. In the lossless case, the response $\boldsymbol{R}_U$ of TL section may be described in the form of ABCD matrix:

$$\boldsymbol{R}_U = \begin{bmatrix} cos(\theta) & jZ_C sin(\theta) \\ \frac{j}{Z_C} sin(\theta) & cos(\theta) \end{bmatrix} \tag{1}$$

The performance of a distributed TL section may be mirrored at the given operating frequency by its corresponding SWRS section in the form of T-type distributed-element circuit, which is composed of interconnected high-impedance Z_H and stepped-impedance sections with low-impedance Z_L stub. Realization of SWRS in such a configuration is particularly attractive due to its considerable slow-wave

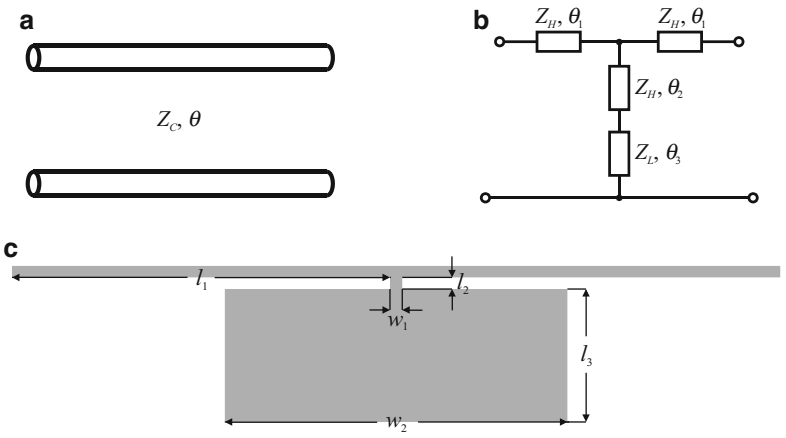

Fig. 4 Various models of a component: (**a**) distributed-element model of TL; (**b**) distributed model of T-type SWRS structure; (**c**) microstrip model of T-type SWRS—parameters w_1, w_2, and l_2 are set based on technology limitations

properties, as well as great usefulness for circuit miniaturization [69, 74, 75]. A conceptual illustration of a TL section and its interchangeable SWRS (both the composite and microstrip realizations) is shown in Fig. 4.

The response of T-type SWRS may be described by the following set of equations:

$$\boldsymbol{R}_T = \begin{bmatrix} cos(\theta_1) & jZ_H sin(\theta_1) \\ \frac{j}{Z_H} sin(\theta_1) & cos(\theta_1) \end{bmatrix} \begin{bmatrix} 1 & 0 \\ \frac{j}{Z_1} & 1 \end{bmatrix} \begin{bmatrix} cos(\theta_1) & jZ_H sin(\theta_1) \\ \frac{j}{Z_H} sin(\theta_1) & cos(\theta_1) \end{bmatrix} \tag{2}$$

$$Z_1 = Z_H \frac{Z_2 + jZ_H tan(\theta_2)}{Z_H + jZ_2 tan(\theta_2)} \tag{3}$$

$$Z_2 = Z_H \frac{Z_L}{jtan(\theta_3)} \tag{4}$$

where θ_1 stands for the electrical length of a high-impedance section, θ_2 and θ_3 denote electrical length of a high-impedance interconnection between the Z_H line and the low-impedance stub, respectively. One should note that parameters Z_H, Z_L and θ_2 may be determined a priori based on technology limitations of microstrip line circuits (minimal/maximal values of line length/width allowed for fabrication) [69]. Parameters θ_1 and θ_3 may be found numerically by solving $\boldsymbol{R}_U = \boldsymbol{R}_T$ for the given operational frequency (parameters Z_C and θ of UTL section are known). Subsequently, geometrical dimensions of SWRS are calculated using general microstrip equations [17].

Although the designed SWRS may be directly utilized for a construction of an unconventional circuit, its shape may not be optimal for some applications. Therefore, Z_H and Z_L sections of the cell may be manually formed—assuming preservation of their electrical properties—to fulfill the specified requirements regarding circuit functionality (e.g., compact size of hybrid couplers [74] or Butler matrices [76]). A more detailed explanation of the knowledge-based construction of SWRS can be found in [72].

3 Surrogate-Based Design and Optimization of Complex Circuits

Design and optimization of unconventional circuits with enhanced functionality is clearly a complex process that involves not only engineering knowledge, but also considerable computational resources. The cost-related issues may be partially alleviated by means of surrogate-based optimization. Here, we discuss a NSM methodology, which is suitable for the design of complex microstrip circuits with SWRS perturbations. We also demonstrate the performance of the NSM technique as well as its advantages over conventional space mapping modeling and optimization.

3.1 Surrogate-Based Optimization

The design of microwave/RF circuit driven by surrogate-based optimization algorithm requires two representations of the same microwave structure at different levels of fidelity. Let $\boldsymbol{R}_f(x)$ be a response vector of a high-fidelity EM model of a complex microwave/RF structure with enhanced functionality, whereas the vector $\boldsymbol{x}$ denotes independent design parameters of the respective circuit. Unfortunately, $\boldsymbol{R}_f$ model is computationally too expensive to be directly used in the numerical optimization process [77]. Instead, a physics-based low-fidelity model $\boldsymbol{R}_s$ in the form of equivalent circuit representation of the respective structure may be—upon suitable correction—utilized to reduce the computational cost of structure optimization. For the sake of brevity, we omit details regarding construction of surrogate model using circuit representation. A comprehensive explanation of this process is available in literature (e.g., [48, 78, 79]).

The design process of microwave/RF circuits may be formulated as a nonlinear minimization problem of the following form:

$$\mathbf{x}^* = \arg\min_{\mathbf{x}} U\left(\mathbf{R}_f(\mathbf{x})\right) \tag{5}$$

where U is a scalar merit function (e.g., a minimax function with upper and lower specifications) that implements given design specifications. Vector $\boldsymbol{x}^*$ is the optimal design to be determined. A high-computational cost of a single EM simulation makes the utilization of conventional optimization to handle (5) impractical, because both gradient-based (e.g., Quasi-Newton [28]) and derivative-free (pattern search [80], genetic algorithms [81]) methods usually require a substantial number of objective function (and thus, high-fidelity model) evaluations. In order to reduce the CPU expense, a direct optimization of a computationally expensive model may be replaced by the following iterative procedure [24, 82]:

$$\mathbf{x}^{(i+1)} = \arg\min_{\mathbf{x}} U\left(\mathbf{R}_s^{(i)}(\mathbf{x})\right) \tag{6}$$

that generates a sequence of approximate solutions $\boldsymbol{x}^{(i)}$ ($i = 0, 1, \ldots$) to the original design problem of (5). The surrogate model at iteration i, $\boldsymbol{R}_s{}^{(i)}$, is constructed from the low-fidelity model so that the misalignment between $\boldsymbol{R}_s{}^{(i)}$ and the fine model is reduced using so-called parameter extraction process. The latter is a nonlinear minimization problem by itself [36]. A conceptual flow of SBO is shown in Fig. 5.

For a well working SBO algorithm, only a few iterations of (6) are necessary to find a satisfactory solution. Also, the fine model is typically evaluated only

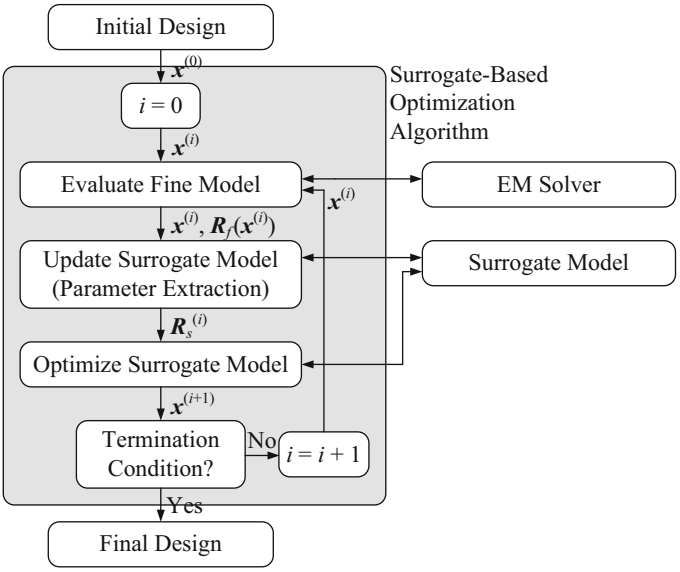

Fig. 5 A conceptual flow of surrogate-based optimization: the optimization burden is shifted to the computationally cheap surrogate model which is updated and re-optimized at each iteration of the main optimization loop. High-fidelity EM simulation is only performed once per iteration to verify the design produced by the surrogate model and to update the surrogate itself. The number of iterations for a well-performing SBO algorithm is substantially smaller than for conventional techniques

once per iteration [83]. However, conventional SBO algorithms—particularly space mapping—suffer from convergence problems or relatively large number of EM model evaluations necessary to conclude the process, if complex microwave/RF designs are considered. These difficulties are alleviated here using a NSM approach.

3.2 NSM Modeling

The NSM technique [51] is a two-level modeling methodology, with the first (inner) space mapping layer applied at the level of component (a so-called local model), and the second (outer) layer applied at the level of the entire structure (so-called global model). The purpose of NSM is to improve the generalization capability of the surrogate model and facilitate the parameter extraction process. Consequently the cost of the design optimization process using NSM can be greatly reduced compared to conventional space mapping applied only at the level of the entire structure [51].

Let $\boldsymbol{R}_{f.cell}(\boldsymbol{y})$ and $\boldsymbol{R}_{c.cell}(\boldsymbol{y})$ be responses (here, *S*-parameters) of the high-fidelity (i.e., EM-simulated) and low-fidelity—circuit-simulated—models of the local component (here, SWRS cell). The vector $\boldsymbol{y}$ represents geometry parameters of the cell, whereas $\boldsymbol{R}_f(\boldsymbol{x})$ and $\boldsymbol{R}_s(\boldsymbol{x})$ denote high- and low-fidelity response of the entire microwave/RF structure with $\boldsymbol{x}$ being a corresponding vector of geometrical parameters. In NSM approach the surrogate model of the entire circuit is constructed starting from the component level, i.e., each SWRS surrogate being relevant for circuit functionality enhancements. A surrogate of inner generic component denoted as $\boldsymbol{R}_{s.g.cell}(\boldsymbol{y},\boldsymbol{p}^*)$ stands for a composition of $\boldsymbol{R}_{c.cell}$ and suitable space mapping transformations; the vector $\boldsymbol{p}^*$ denotes the set of extractable space mapping parameters of the model. The space mapping surrogate $\boldsymbol{R}_{s.cell}$ of a SWRS component is obtained as

$$\mathbf{R}_{s.cell}(\mathbf{y}) = \mathbf{R}_{s.g.cell}(\mathbf{y}, \mathbf{p}^*) \tag{7}$$

The parameter vector $\boldsymbol{p}^*$ is obtained by solving the following nonlinear parameter extraction process

$$\mathbf{p}^* = \arg\min_{\mathbf{p}} \sum_{k=1}^{N_{cell}} \left|\left|\mathbf{R}_{s.g.cell}\left(\mathbf{y}^{(k)}, \mathbf{p}\right) - \mathbf{R}_f\left(\mathbf{y}^{(k)}\right)\right|\right| \tag{8}$$

where vectors $\boldsymbol{y}^{(k)}$, $(k = 1, \ldots, N_{cell})$ denote the training (or base) solutions obtained using a so-called star-distribution scheme [36]. A base obtained using star-distribution method is composed of $N_{cell} = 2d + 1$, where d is design space dimensionality (i.e., a number of independent design variables). Although local generic surrogate of each SWRS depends on much smaller number of parameters than the structure optimized using conventional space mapping technique (usually up to a few independent variables rather than a few dozen [51]), it exploits a combination of various space mapping methods (c.f. Sect. 3.3) [41]. Therefore,

a local surrogate model $\boldsymbol{R}_{s.cell}$ implemented within a global model of the whole microwave/RF circuit should be valid for the entire range of parameters $\boldsymbol{y}$.

A generic space mapping surrogate of the entire unconventional circuit denoted by $\boldsymbol{R}_{s.g}(\boldsymbol{x},\boldsymbol{P})$ is composed of the local models of individual SWRS cells:

$$R_{s.g}(x, P) = R_{s.g}\left(\left[y_1; \ldots; y_p\right], P\right) = F\left(R_{s.g.cell}\left(y_1, p^*\right), \ldots, R_{s.g.cell}\left(y_p, p^*\right), P\right) \tag{9}$$

where F realizes a sufficient connection between respective sections of a structure with enhanced functionality. Vector $\boldsymbol{x}$ represents a concatenation of component parameter vectors $\boldsymbol{y}_k$, while vector $\boldsymbol{P}$ stands for space mapping parameters at the outer level. One should note that $\boldsymbol{P}$ is usually defined as perturbations (with respect to $\boldsymbol{p}^*$) of selected space mapping parameters of individual components.

The outer space mapping level is applied to the global model $\boldsymbol{R}_{s.g}(\boldsymbol{x},\boldsymbol{P})$, so that the final surrogate $\boldsymbol{R}_s{}^{(i)}$ utilized in the ith iteration of the SBO scheme (6) is defined as follows

$$\mathbf{R}_s^{(i)}(\mathbf{x}) = \mathbf{R}_{s.g}\left(\mathbf{x}^{(i)}, \mathbf{P}^{(i)}\right) \tag{10}$$

where

$$\mathbf{P}^{(i)} = \arg\min_{\mathbf{P}} \| \mathbf{R}_{s.g}\left(\mathbf{x}^{(i)}, \mathbf{P}\right) - \mathbf{R}_f\left(\mathbf{x}^{(i)}\right) \| \tag{11}$$

It should be emphasized that the number of parameters in $\boldsymbol{P}$ is much smaller than the combined number of space mapping parameters of SWRS components (i.e., multiple copies of a vector $\boldsymbol{p}^*$). This is normally sufficient because the inner space mapping layer already provides good alignment between the $\boldsymbol{R}_{s.cell}$ and $\boldsymbol{R}_{f.cell}$ so that the role of (10), (11) is mainly to account for possible interactions between SWRS components that are considered by the composing function F. The algorithm may be summarized as follows (see Fig. 6 for conceptual illustration):

1. Construct circuit model $\boldsymbol{R}_{c.cell}$ of the nth SWRS component;
2. Obtain inner space mapping surrogate $\boldsymbol{R}_{s.cell}$ of nth SWRS by performing multipoint extraction of $\boldsymbol{p}^*$ parameters;
3. If $n < N$ go to 1;
4. Utilize N $\boldsymbol{R}_{s.cell}$ components to construct a generic space mapping surrogate $\boldsymbol{R}_{s.g}(\boldsymbol{x},\boldsymbol{P})$ of an unconventional microwave/RF circuit;
5. Utilize SBO scheme for the determination of desired functionality at the output space mapping level.

3.3 Surrogate Model Construction

Multipoint parameter extraction utilized for a construction of a reliable local model of SWRS component requires a combination of various space mapping techniques to

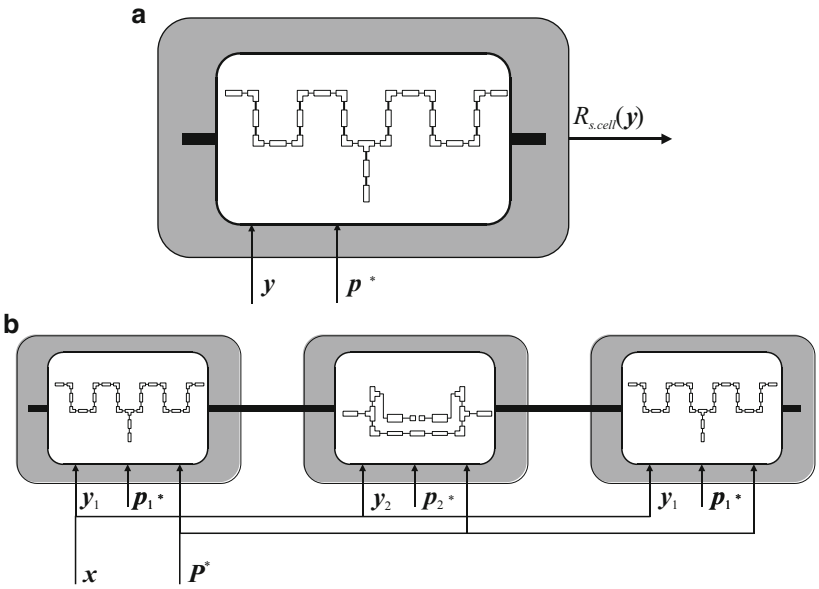

Fig. 6 The concept of nested space mapping (NSM): (**a**) local space mapping model of SWRS component. Extractable parameters $\boldsymbol{p}^*$ are optimized to match the circuit $\boldsymbol{R}_{s.cell}(\boldsymbol{y})$ and $\boldsymbol{R}_{f.cell}(\boldsymbol{y})$ within solution space; (**b**) global space mapping model composed of two SWRS components. Once extractable parameters $\boldsymbol{p}^*_{(1,2)}$ are set they are reused in global model. Vector of design parameters $\boldsymbol{x}$ is optimized to obtain desired specification

achieve desired generalization. The inner space mapping layer is constructed using the following relation:

$$\mathbf{R}_{s.g.cell}\left(\mathbf{y},\mathbf{p}\right) = \mathbf{R}_{c.F}\left(\mathbf{B}\cdot\mathbf{x}+\mathbf{c},\mathbf{p}_I\right) \tag{12}$$

where $\boldsymbol{B}$ and $\boldsymbol{c}$ are input space mapping parameters (a diagonal matrix $\boldsymbol{B}$ is utilized), $\boldsymbol{p}_I$ are implicit space mapping (ISM) parameters (a substrate parameters of individual microstrip subsection of SWRS component, specifically, dielectric permittivity and the substrate heights). Additionally, a frequency scaling $\boldsymbol{R}_{c.F}$ of low-fidelity model aimed at evaluation of the $\boldsymbol{R}_c$ model across the frequency band of interest, is performed. The frequency-scaled model $\boldsymbol{R}_{c.F}(\boldsymbol{y})$ corresponding to $\boldsymbol{R}_c(\boldsymbol{y}) = [R_c(\boldsymbol{y},\omega_1)\ R_c(\boldsymbol{y},\omega_2)\ \ldots\ R_c(\boldsymbol{y},\omega_m)]^T$ is defined as flows:

$$\mathbf{R}_{c.F}\left(\mathbf{y},\mathbf{p}\right) = [R_c\left(\mathbf{y},\, f_0+\omega_1\cdot f_1\right) \quad R_c\left(\mathbf{y},\, f_0+\omega_2\cdot f_1\right) \quad \ldots \quad R_c\left(\mathbf{y},\, f_0+\omega_m\cdot f_1\right)]^T \tag{13}$$

where f_0, f_1 are extractable scaling parameters. Technique is especially useful for correction of frequency misalignment between low- and high-fidelity models of

the SWRS component [51]. An exemplary inner space mapping layer of SWRS component $\boldsymbol{R}_{s.cell}(\boldsymbol{y}, \boldsymbol{p})$ and its corresponding high-fidelity model $\boldsymbol{R}_{f.cell}(\boldsymbol{y})$ are shown in Fig. 7.

3.4 Generalization Capability of NSM

The most notable advantage of NSM technique lies in good generalization capability of the global NSM surrogate $\boldsymbol{R}_{s.g}$, which is achieved by global accuracy of each local SWRS model $\boldsymbol{R}_{s.cell}$ utilized for a construction of unconventional microwave/RF circuit. A typical modeling accuracy of an exemplary SWRS cell (see Fig. 7) after multipoint parameter extraction is illustrated in Fig. 8. A comparison of global NSM surrogate for an exemplary structure—in the form of unconventional

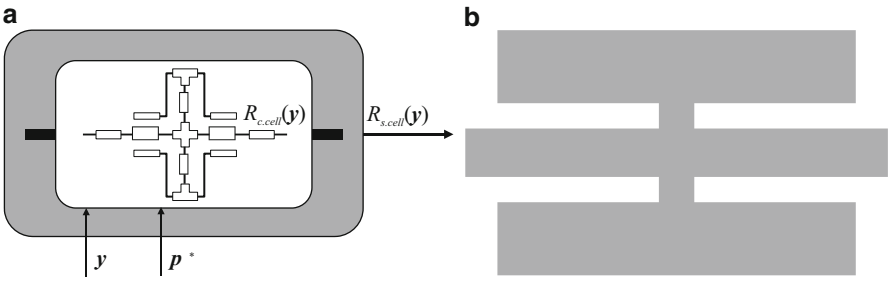

Fig. 7 An exemplary SWRS component: (**a**) coarse model $\boldsymbol{R}_{c.cell}(\boldsymbol{y})$ within inner space mapping layer $\boldsymbol{R}_{s.cell}(\boldsymbol{y})$; (**b**) high-fidelity EM model $\boldsymbol{R}_{f.cell}(\boldsymbol{y})$

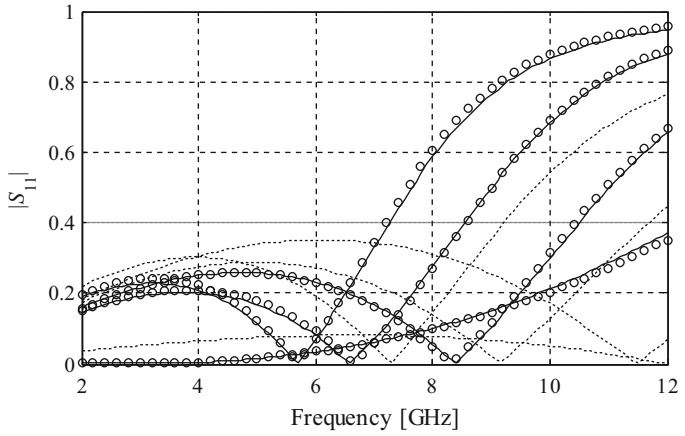

Fig. 8 NSM modeling of SWRS component. Responses at the selected test designs: coarse model (*dotted line*), fine model (*solid line*), NSM surrogate after multipoint parameter extraction (*open circle*). The plots indicate very good approximation capability of the surrogate

Fig. 9 Geometry of an exemplary matching transformer composed by cascading three SWRS sections of Fig. 7

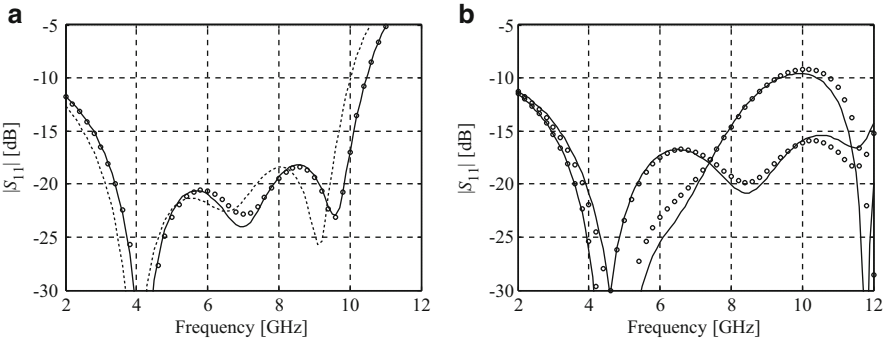

Fig. 10 NSM modeling of a matching transformer of Fig. 9: (**a**) high-fidelity model response (*solid line*), NSM surrogate before parameter extraction (*dotted line*) and NSM surrogate after parameter extraction (*open circle*); (**b**) visualization of excellent generalization of NSM surrogate (*open circle*) extracted at random designs. Corresponding high-fidelity model responses (*solid line*) are also provided

matching transformer of Fig. 9—before and after parameter extraction step (10) is shown in Fig. 10. One should emphasize that $\boldsymbol{R}_{s.g}$ model matches its high-fidelity counterpart even before parameter extraction step. Therefore, parameter extraction is aimed only at addressing the interactions (i.e., couplings) between respective SWRS components that are not accounted by the $\boldsymbol{R}_{s.cell}$ models.

For a comparison purpose, an exemplary transformer of Fig. 9 is also designed using conventional space mapping modeling (i.e., correction of its low-fidelity model $\boldsymbol{R}_c$). The process of circuit design in such a setup is considerably more complex because (1) the low-fidelity model of the entire unconventional microwave/RF circuit is much less accurate than $\boldsymbol{R}_{s.g}$ (cf. Fig. 11a), (2) a large number of space mapping parameters with considerable range of variation is required, (3) the parameter extraction process is more challenging and time consuming, and (4) generalization capability of the model is poor (cf. Fig. 11b).

Sufficient accuracy of the underlying low-fidelity model and good generalization capability of the surrogate are essential for fast convergence of the SBO optimization process (6) [51]. The NSM model exhibits both aforementioned features (here, the global model $\boldsymbol{R}_{s.g}$ is formally a low-fidelity model for (6)), which results in not only rapid, but also accurate design of complex microwave/RF circuits with enhanced functionality.

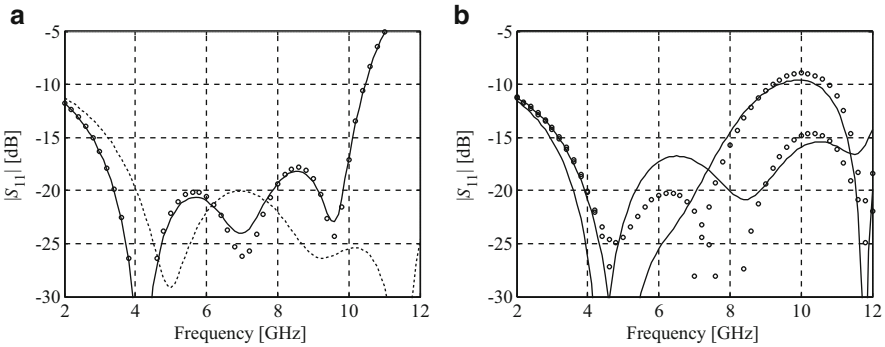

Fig. 11 Conventional space mapping modeling of a matching transformer of Fig. 9: (**a**) high-fidelity model response (*solid line*), SM surrogate before (*dotted line*) and after parameter extraction (*open circle*); (**b**) visualization of poor generalization capability of a surrogate (*open circle*) extracted at random designs. Corresponding high-fidelity model responses (*solid line*) are also provided

4 Case Studies

In this section, we present verification examples for the design of complex microwave/RF circuits using NSM methodology of Sect. 3. The technique is validated using a four-section ultra-wideband matching transformer with 16 independent design variables, a 15-variable broadband three section matching transformer, and a miniaturized rat-race coupler with a total of ten designable parameters. Unconventional properties of illustrative circuits are obtained by implementation of SWRS components using both the database approach of Sect. 2.2 and knowledge-based design of complementary SWRS explained in Sect. 2.3. A comparison of the NSM technique with sequential space mapping (SSM) and implicit space mapping (ISM) methods is also provided.

4.1 Design of Ultra-Wideband Four-Section Matching Transformer

Consider a four-section microstrip matching transformer (MT). The structure is aimed to mimic the functionality of a conventional MT, i.e., (1) match a 50 Ω line to a 130 Ω load, and (2) provide a reflection coefficient $|S_{11}| \leq -15$ dB within 3.1–10.6 GHz frequency band of interest (ultra-wideband structure). A circuit is considered to operate on Taconic RF-35 dielectric substrate ($\varepsilon_r = 3.5$, $\tan\delta = 0.0018$, $h = 0.762$).

A prototype circuit satisfying design specifications regarding reflection and matching properties is constructed using binomial design expressions [17] resulting

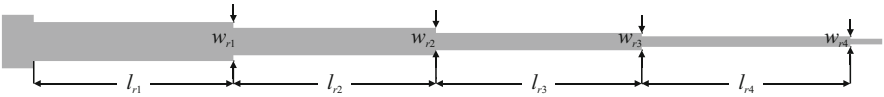

Fig. 12 Geometry of a conventional four-section MT

in a cascade of four quarter-wavelength ($\theta = 90°$ at $f_0 = 6.65$ GHz) TL sections described by the following vector of characteristic impedances $Z_C = [53.1\ 67.4\ 96.4\ 122.5]^T\ \Omega$. Subsequently, physical dimensions of the MT: $\boldsymbol{x}_r = [w_{r1}\ w_{r2}\ w_{r3}\ w_{r4}\ l_{r1}\ l_{r2}\ l_{r3}\ l_{r4}]^T$ are calculated using general equations for microstrip lines and slightly tuned. The design parameters of the reference structure (see Fig. 12) are $\boldsymbol{x}_r = [1.2\ 0.9\ 0.5\ 0.3\ 6.6\ 6.8\ 6.7\ 7.0]^T$. Moreover, variables $l_{r0} = 10$, $w_{ri0} = 1.7$, and $w_{ro0} = 0.18$ denote size of 50 and 130 Ω lines (all dimensions in mm).

The reference MT is characterized by a very simple geometry that allows for its decomposition into four TL sections (cf. Sect. 2.1). Furthermore, similarities between consecutive cells indicate that they might be substituted with one versatile SWRS component. An appropriate structure may be found using database approach described in Sect. 2.2. A desired SWRS is intended to mimic a range of characteristic impedances Z_C with preservation of electrical length around 90°. A double-T-type SWRS constituted by a vector of four independent design parameters: $\boldsymbol{y} = [l_1\ l_2\ w_1\ w_2]^T$ (dimensions $l_3 = 0.2$ and $w_3 = 0.2$ are fixed) is sufficient to fulfill our needs [73]. One should emphasize that due to technology limitations (i.e., minimum feasible width of the SWRS lines and the gaps between them equal to 0.1 mm), acceptable structure dimensions are defined by the following lower/upper $\boldsymbol{l}/\boldsymbol{u}$ bounds: $\boldsymbol{l} = [0.1\ 1\ 0.1\ 0.1]^T$ and $\boldsymbol{u} = [1\ 5\ 1\ 1]^T$. The high-fidelity model $\boldsymbol{R}_{f.cell}$ of the double-T-type SWRS (∼200,000 mesh cells and evaluation time of 60 s) is implemented in CST Microwave Studio [84], whereas its low-fidelity model $\boldsymbol{R}_{c.cell}$ is constructed in Agilent ADS circuit simulator [85].

The inner layer model $\boldsymbol{R}_{s.cell}$ of the chosen double-T-type SWRS component is constituted by 16 space mapping parameters, including: eight input space mapping (four $\boldsymbol{B} = diag([B_1\ B_2\ B_3\ B_4]^T)$ and four $\boldsymbol{c} = [c_1\ c_2\ c_3\ c_4]^T$ parameters), six ISM (three various substrate heights and permittivity parameters $\boldsymbol{p}_I = [h_1\ h_2\ h_3\ \varepsilon_1\ \varepsilon_2\ \varepsilon_3]^T$), and two frequency scaling (f_0 and f_1) ones. A multipoint parameter extraction based on star-distribution scheme (c.f. Sect. 3.2) has been conducted to achieve $\boldsymbol{R}_{s.cell}$ model generalization within predefined lower/upper bounds. A comparison of the component characteristics before and after multipoint parameter extraction is shown in Fig. 8, whereas a double-T-type structure with highlighted geometrical and space mapping parameters is shown in Fig. 13.

A global model $\boldsymbol{R}_{s.g}$ of the unconventional MT has been constructed using a cascade connection of $\boldsymbol{R}_{s.cell}$ models of the double-T-type component. Subsequently, the high-fidelity model of the structure has been prepared in CST Microwave Studio (∼1,060,000 mesh cells and average simulation time 10 min). The initial set of parameters is $\boldsymbol{x} = [0.55\ 3.75\ 0.65\ 0.35\ 0.55\ 3.75\ 0.65\ 0.35\ 0.55\ 3.75\ 0.65\ 0.35\ 0.55\ 3.75\ 0.65\ 0.35]^T$. Subsequently, the circuit has been optimized using

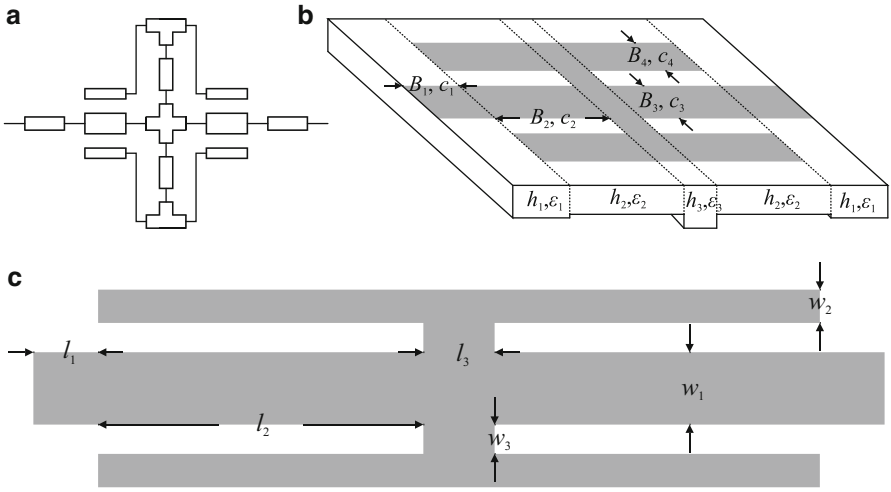

Fig. 13 A double-T-type SWRS component: (**a**) low-fidelity $\boldsymbol{R}_{c.cell}$ model; (**b**) conceptual visualization of the inner layer model $\boldsymbol{R}_{s.cell}$ with highlighted extractable parameters; (**c**) topology of $\boldsymbol{R}_{f.cell}$ model with highlighted geometrical parameters

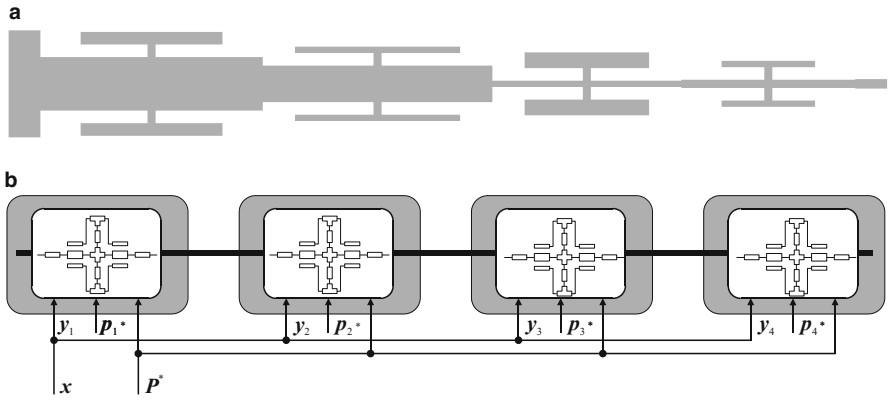

Fig. 14 An unconventional MT composed of cascade connection of double-T-type SWRS components [51]: (**a**) geometry of an optimized structure; (**b**) schematic diagram of SWRS interconnections

the NSM technique of Sect. 3. The final design of complex MT is denoted by vector $\boldsymbol{x} = [1.0\ 3.52\ 0.85\ 0.2\ 0.8\ 4.1\ 0.58\ 0.1\ 0.8\ 3.09\ 0.1\ 0.25\ 1\ 2.32\ 0.13\ 0.1]^T$. Figure 14 illustrates geometry of the structure as well as schematic diagram of $\boldsymbol{R}_{s.cell}$ interconnections.

The final design of the unconventional MT is obtained after three iterations of the NSM algorithm. The structure fulfills all assumed design specifications: (1) it provides 50–130 Ω matching as well as (2) $|S_{11}| \leq -16.2$ dB within band of interest.

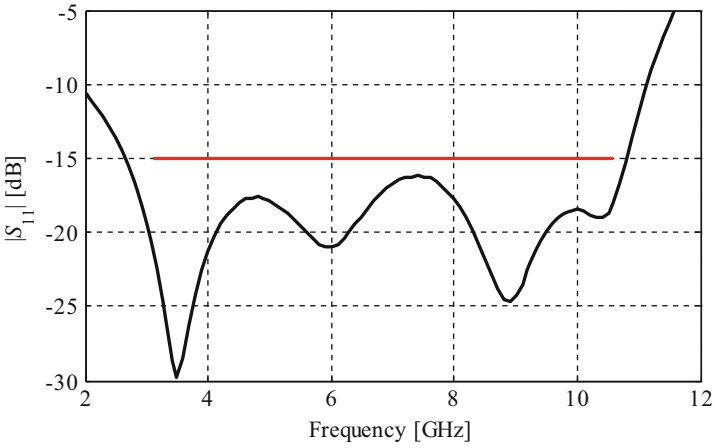

Fig. 15 Reflection response of the optimized unconventional MT

Moreover, the operational bandwidth of the circuit for reflection below −15 dB is 2.7–10.8 GHz, which is 15 % broader than assumed one. Figure 15 presents simulated characteristics of the unconventional MT. One should emphasize that the number of the outer layer SM parameters $\boldsymbol{P}$ is much smaller than the combined set of SM parameters for the inner layer (14 vs. 64 for the considered structure) as only frequency scaling and selected implicit SM parameters are used. Reduction of the number of parameters (introduced by excellent generalization capability of NSM) considerably speeds up the design process.

The cost of inner space mapping model preparation corresponds to nine $\boldsymbol{R}_{f.cell}$ model evaluations for multi parameter extraction step, while determination of the final design required only three evaluations of the $\boldsymbol{R}_f$ model. The accumulated cost of $\boldsymbol{R}_{s.cell}$ and $\boldsymbol{R}_{s.g}$ models evaluations corresponds to about 0.2 $\boldsymbol{R}_f$ evaluations, thus the total aggregated cost of the unconventional MT design using the NSM technique is about 40 min. For the sake of comparison, the design process of MT has been also conducted by means of ISM [47] and SSM [27] techniques resulting in considerably higher computational cost or failure of algorithms. Additionally, a direct optimization of the transformer using pattern search method [80] was carried out. The algorithm failed at seeking for desired circuit dimensions and has been terminated after 500 iterations. A detailed comparison of the computational costs of mentioned optimization techniques is provided in Table 1.

4.2 Design of a Broadband Three Section Matching Transformer

Consider a microstrip MT composed of three sections. The structure is aimed to mimic the functionality of a conventional TL-based MT, i.e., (1) match a 50 Ω

Table 1 Four-section unconventional MT: design and optimization cost

	Optimization algorithm			
Model evaluations	NSM	ISM	SSM	Direct search
SWRS $\boldsymbol{R}_{s.cell}$	$0.1 \times \boldsymbol{R}_f$	N/A	N/A	N/A
SWRS $\boldsymbol{R}_{f.cell}$	$0.6 \times \boldsymbol{R}_f$	N/A	N/A	N/A
MT low-fidelity $\boldsymbol{R}_s$	$0.1 \times \boldsymbol{R}_f$	$5.1 \times \boldsymbol{R}_f$	$1.7 \times \boldsymbol{R}_f$	N/A
MT high-fidelity $\boldsymbol{R}_f$	3	7	10[a]	500[b]
Total cost	$3.8 \times \boldsymbol{R}_f$	$12.1 \times \boldsymbol{R}_f$	$11.7 \times \boldsymbol{R}_f$	500[b] $\times \boldsymbol{R}_f$
Total cost [min]	38	121	N/A	5,000

[a]The algorithm started diverging and was terminated after ten iterations
[b]The algorithm failed to find a geometry satisfying performance specifications

line to 130 Ω load and (2) obtain reflection $|S_{11}| \leq -15$ dB within 1–3.5 GHz frequency band of interest. Additionally, circuit is intended to offer at least 50 % length diminution in comparison to the conventional one. A structure is considered to work on Taconic RF-35 dielectric substrate ($\varepsilon_r = 3.5$, $\tan\delta = 0.0018$, $h = 0.762$).

A binomial design expressions are utilized for a construction of a sufficient prototype circuit in the form of a cascade connection of three TL sections with $\theta = 90°$ for the given operating frequency of $f_0 = 2.25$ GHz. The characteristic impedances of the prototype circuit are represented by vector $Z_C = [56.3\ 80.6\ 115.4]^T$ Ω, while physical dimensions: $\boldsymbol{x}_r = [w_{r1}\ w_{r2}\ w_{r3}\ l_{r1}\ l_{r2}\ l_{r3}]^T$ of the MT are calculated using general microstrip equations. Subsequently, the circuit is tuned to match the design requirements resulting in the following variables: $\boldsymbol{x}_r = [1.09\ 0.64\ 0.34\ 20\ 21.7\ 23.6]^T$. Moreover, $l_{r0} = 10$, $w_{ri0} = 1.7$, and $w_{ro0} = 0.18$ denote dimensions of 50 and 130 Ω lines (all dimensions in mm).

The reference structure has been decomposed into three TL sections (cf. Sect. 2.1). Moreover, a database approach of Sect. 2.2 has been utilized for the determination of SWRS component that is versatile enough to substitute all TL sections. Therefore, a desired SWRS is intended to mimic their Z_C parameters for electrical length θ being around 90°. A SWRS in the form of C-type component is suitable to fulfill the specification [73]. The structure is represented by the following vector of geometrical parameters: $\boldsymbol{y} = [w_1\ w_2\ w_3\ l_1\ l_2]^T$. The lower/upper bounds imposed by technology limitations of circuit realization in microstrip technology (i.e., minimal feasible width of SWRS lines and gaps between them equal to 0.1) are set to: $\boldsymbol{l} = [0.1\ 0.1\ 0.1\ 5\ 0.1]^T$ and $\boldsymbol{u} = [2\ 2\ 0.5\ 10\ 0.5]^T$. The high-fidelity model $\boldsymbol{R}_{f.cell}$ of C-type SWRS component is implemented in CST Microwave Studio. An average evaluation time of the model is 60 s (∼330,000 mesh cells). The low-fidelity model $\boldsymbol{R}_{c.cell}$ of the structure is prepared in Agilent ADS circuit simulator.

Eighteen space mapping parameters of the inner layer model $\boldsymbol{R}_{s.cell}$ include: ten input space mapping (five $\boldsymbol{B} = \text{diag}([B_1\ B_2\ B_3\ B_4\ B_5]^T)$ and five $\boldsymbol{c} = [c_1\ c_2\ c_3\ c_4\ c_5]^T$ parameters), six ISM (three various substrate heights and three permittivity

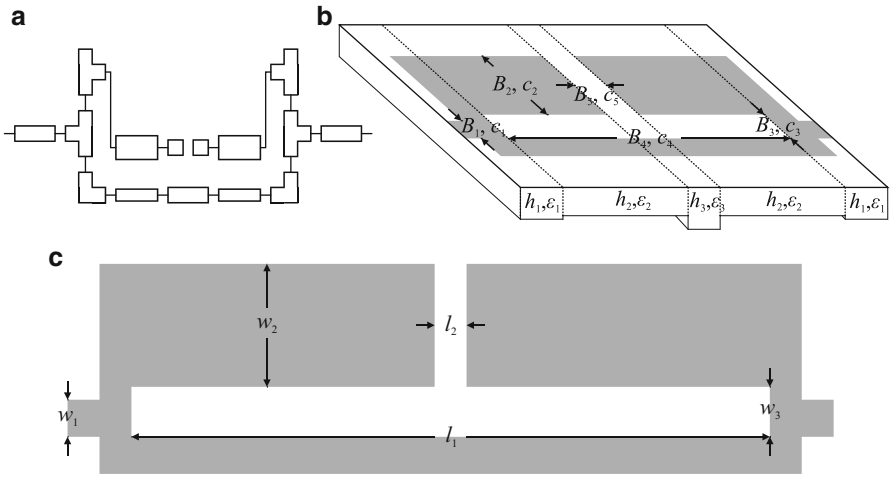

Fig. 16 A C-type SWRS component: (**a**) low-fidelity $\boldsymbol{R}_{c.cell}$ model; (**b**) conceptual visualization of inner layer model $\boldsymbol{R}_{s.cell}$ with highlighted 16 extractable parameters (except frequency scaling); (**c**) topology of $\boldsymbol{R}_{f.cell}$ model with highlighted five geometrical parameters

parameters $\boldsymbol{p}_I = [h_1\ h_2\ h_3\ \varepsilon_1\ \varepsilon_2\ \varepsilon_3]^T$), and two frequency scaling (f_0 and f_1) ones. A star-distribution scheme of Sect. 3.2 has been utilized for multipoint parameter extraction of the $\boldsymbol{R}_{s.cell}$ model. Figure 16 illustrates the structure with the emphasis on its geometrical and extractable parameters.

A cascade connection of three $\boldsymbol{R}_{s.cell}$ models of the C-type SWRS component has been utilized for a construction of a global $\boldsymbol{R}_{s.g}$ model of unconventional MT. A high-fidelity model $\boldsymbol{R}_f$ of the entire structure has been implemented in CST Microwave Studio (∼1,400,000 mesh cells and average simulation time 18 min). The initial set of parameters is: $\boldsymbol{x} = [0.2\ 1\ 0.2\ 4\ 0.2\ 0.2\ 1\ 0.2\ 4\ 0.2\ 0.2\ 1\ 0.2\ 4\ 0.2]^T$. Subsequently, NSM methodology of Sect. 3 has been utilized for optimization of the structure resulting in the following vector of design parameters: $\boldsymbol{x} = [1.21\ 0.18\ 10\ 0.3\ 0.5\ 1.5\ 0.2\ 8.98\ 0.3\ 0.19\ 0.97\ 0.15\ 10\ 0.3\ 0.15]^T$. Geometry of unconventional structure and a schematic diagram of $\boldsymbol{R}_{s.cell}$ interconnections are shown in Fig. 17.

The unconventional MT that offers over 51 % length reduction (length of 31.9 mm) in comparison to conventional structure (length of 65.3 mm) and reflection $|S_{11}| \leq -17$ within band of interest is obtained using only three iterations of NSM algorithm. Furthermore, $|S_{11}| \leq -15$ dB of an abbreviated circuit is obtained within 0.9–3.6 GHz frequency band. Similarly to the results of Sect. 4.1, the width of an unconventional MT is slightly greater than of conventional one. Figure 18 shows comparison of the reflection characteristics of the conventional and the abbreviated MT.

A total design and optimization cost of the structure, including eleven $\boldsymbol{R}_{f.cell}$ model evaluations during generation of the inner space mapping layer, three $\boldsymbol{R}_f$ model simulations for optimization of unconventional MT circuit, and evaluations

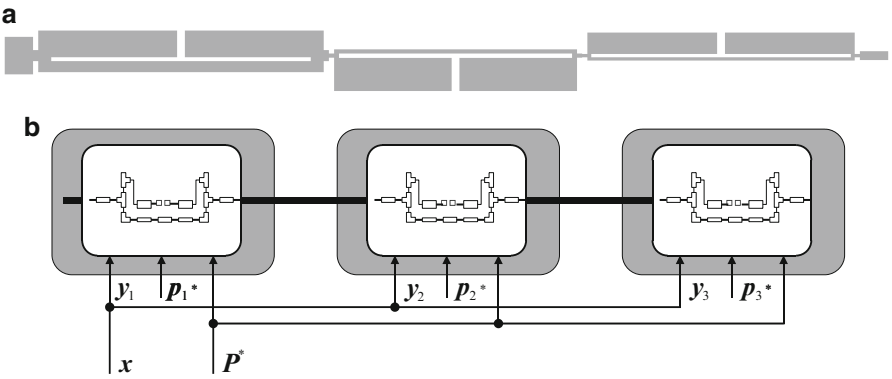

Fig. 17 An abbreviated MT composed of four C-type SWRS components: (**a**) geometry of an optimized structure; (**b**) schematic diagram of SWRS cascade connection

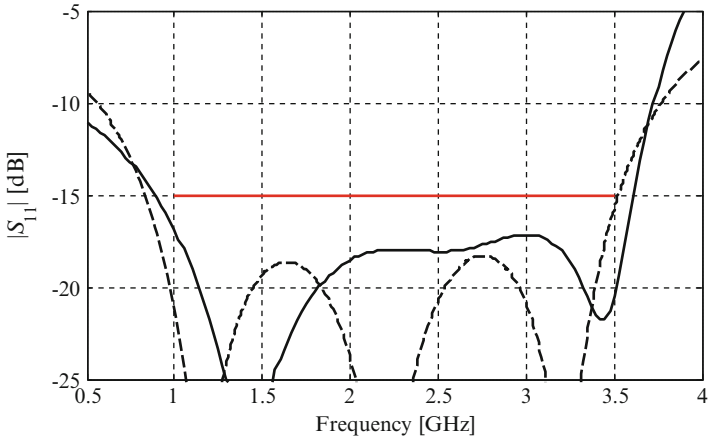

Fig. 18 Reflection characteristics of the conventional (*dashed line*) and abbreviated (*solid line*) MT

of surrogate models ($\boldsymbol{R}_{s.g}$ and $\boldsymbol{R}_{s.cell}$) corresponds to about 0.5 $\boldsymbol{R}_f$ model simulations (∼1.2 h). Alternative techniques including ISM and SSM as well as direct optimization driven by pattern search algorithm have been also utilized for the design and optimization of abbreviated MT. SSM and ISM requires twice as many iterations as NSM approach, while direct optimization required 520 iterations to complete, which turns the method virtually impractical for such circuits. A detailed comparison of the methods in terms of iterations is collected in Table 2.

Table 2 An abbreviated three section MT: design and optimization cost

	Optimization algorithm			
Model evaluations	NSM	ISM	SSM	Direct search
SWRS $\boldsymbol{R}_{s.cell}$	$0.2 \times \boldsymbol{R}_f$	N/A	N/A	N/A
SWRS $\boldsymbol{R}_{f.cell}$	$0.6 \times \boldsymbol{R}_f$	N/A	N/A	N/A
MT low-fidelity $\boldsymbol{R}_s$	$0.3 \times \boldsymbol{R}_f$	$3 \times \boldsymbol{R}_f$	$1.3 \times \boldsymbol{R}_f$	N/A
MT high-fidelity $\boldsymbol{R}_f$	3	7	6	520
Total cost	$4.1 \times \boldsymbol{R}_f$	$10 \times \boldsymbol{R}_f$	$7.3 \times \boldsymbol{R}_f$	$520 \times \boldsymbol{R}_f$
Total cost [h]	1.2	3.2	2.3	149.8

4.3 Design of a Compact Rat-Race Coupler

Our last example is an unconventional rat-race coupler (RRC). The structure is desired to fulfill the following design specifications: (1) at least 20 % bandwidth defined for both isolation $|S_{41}|$ and reflection coefficients $|S_{11}|$ below −20 dB and (2) −3 dB coupling. Both goals are considered for the given operating frequency $f_0 = 1$ GHz. Moreover, the design is intended to achieve at least 80 % of footprint reduction in comparison with conventional rectangle-based RRC. The circuit is desired to operate on Taconic RF-35 dielectric substrate ($\varepsilon_r = 3.5$, $\tan\delta = 0.0018$, $h = 0.762$).

A conventional, equal-split RRC may be constructed using well-known even-odd mode analysis [70]. The reference circuit is composed of six TL sections of characteristic impedance $Z_C = \sqrt{2}\ Z_0\ \Omega$ and electrical length $\theta = 90°$, where $Z_0 = 50\ \Omega$ is the characteristic impedance of feed lines. Moreover, TL sections are interconnected through tee junctions and microstrip bends (see Fig. 2b). Physical dimensions of the conventional structure are represented by a vector: $\boldsymbol{x}_r = [w_{r1}\ l_{r1}]^T$. The dimensions of reference design are: $\boldsymbol{x}_r = [0.87\ 45.8]^T$, while parameters $l_0 = 10$, $w_0 = 1.7$ are fixed to ensure 50 Ω feed (all dimensions in mm). One should emphasize that the design is characterized by a considerable footprint of ∼4,536 mm^2 (47.5 × 95.5 mm^2).

A conventional RRC may be decomposed into six TL sections characterized by the same electrical parameters. Unfortunately, determination of SWRS component for TL replacement by means of database approach prevents sufficient circuit miniaturization. For that reason, we perform a knowledge-based construction of SWRSs (cf. Sect. 2.3) aimed at manual forming of components to maximally utilize interior of the coupler. To satisfy miniaturization requirements, $n = 2$ complementary SWRS components based on T-type topology have been constructed. Both cells are represented by the following vectors of design parameters: $\boldsymbol{y}^{(1)} = [w_{11}\ l_{11}\ l_{21}\ l_{31}\ l_{41}]^T$ and $\boldsymbol{y}^{(2)} = [w_{12}\ l_{12}\ l_{22}\ l_{32}\ l_{42}]^T$. Technology limitations impose the lower/upper bounds of each structure dimensions: $\boldsymbol{l}^{(1)} = [0.2\ 0.2\ 0.2\ 0.2\ 0.2]^T$, $\boldsymbol{u}^{(1)} = [0.5\ 0.5\ 4\ 0.5\ 4]^T$, and $\boldsymbol{l}^{(2)} = [0.2\ 0.2\ 0.2\ 0.2\ 0.2]^T$, $\boldsymbol{u}^{(2)} = [0.5\ 1\ 7\ 0.5\ 7]^T$. The high-fidelity models $\boldsymbol{R}_{f.cell}{}^{(n)}$ of SWRS are both prepared in CST Microwave Studio (∼340,000

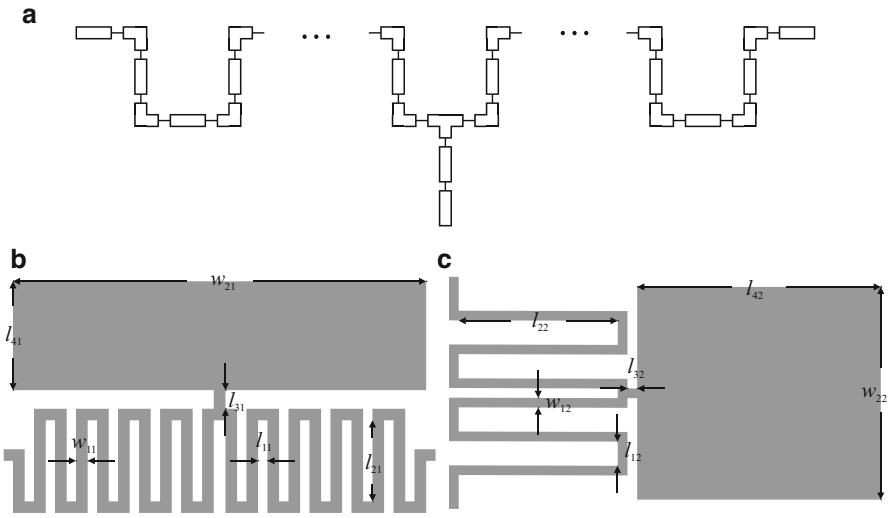

Fig. 19 A T-type SWRS components designed by means of knowledge-based approach: (**a**) general visualization of low-fidelity $\boldsymbol{R}_{c.cell}{}^{(1)}$ and $\boldsymbol{R}_{c.cell}{}^{(2)}$ models; (**b**) topology of $\boldsymbol{R}_{f.cell}{}^{(1)}$ model with highlighted six geometrical parameters ($w_{21} = 18l_{11} + 21w_{11}$); (**c**) topology of $\boldsymbol{R}_{f.cell}{}^{(2)}$ model 6 geometrical parameters are highlighted ($w_{22} = 6l_{12} + 7w_{12}$)

and ∼400,000 mesh cells, as well as 4 and 4.5 min evaluation time for $\boldsymbol{R}_{f.cell}{}^{(1)}$ and $\boldsymbol{R}_{f.cell}{}^{(2)}$ respectively). The low-fidelity models $\boldsymbol{R}_{c.cell}{}^{(n)}$ of both structures are constructed in Agilent ADS circuit simulator. Designs of both components with highlighted geometrical parameters as well as visualization of their circuit models are illustrated in Fig. 19.

A star-distribution design of experiments scheme for training data allocation (cf. Sect. 3.2) has been utilized for a multipoint parameter extraction. Inner space mapping layers of $\boldsymbol{R}_{s.cell}{}^{(1)}$ and $\boldsymbol{R}_{s.cell}{}^{(2)}$ models have been both composed of 18 parameters. The surrogate model responses of both SWRS components before and after multipoint parameter extraction are shown in Fig. 20.

A global model $\boldsymbol{R}_{s.g}$ of compact RRC has been constructed using two $\boldsymbol{R}_{s.cell}{}^{(1)}$ and four $\boldsymbol{R}_{s.cell}{}^{(2)}$ models that substitute TL sections of a conventional circuit. The coupler dimensions are represented by the following vector: $\boldsymbol{x} = [w_{11}\ l_{11}\ l_{21}\ l_{31}\ l_{41}\ w_{12}\ l_{12}\ l_{22}\ l_{32}\ l_{42}]^T$, whereas $w_{10} = 0.75$, $l_{10} = 4.3$, $l_{20} = 0.4$ remain fixed. Moreover, $w_{21} = 18l_{11} + 21w_{11}$ and $w_{22} = 6l_{12} + 7w_{12}$. A high-fidelity model $\boldsymbol{R}_f$ of the structure has been prepared in CST Microwave Studio (∼800,000 mesh cells and average simulation time 75 min per design). The initial design parameters are: $\boldsymbol{x} = [0.2\ 0.2\ 2.5\ 0.2\ 2.5\ 0.2\ 0.2\ 5.0\ 0.2\ 5.0]^T$. A NSM methodology of Sect. 3 has been utilized for optimization of the structure resulting in the following vector of design parameters: $\boldsymbol{x} = [0.24\ 0.26\ 3.35\ 0.28\ 2.04\ 0.25\ 0.29\ 6.52\ 0.29\ 5.63]^T$. Geometry of the unconventional structure and a schematic diagram of $\boldsymbol{R}_{s.g}$ are shown in Fig. 21.

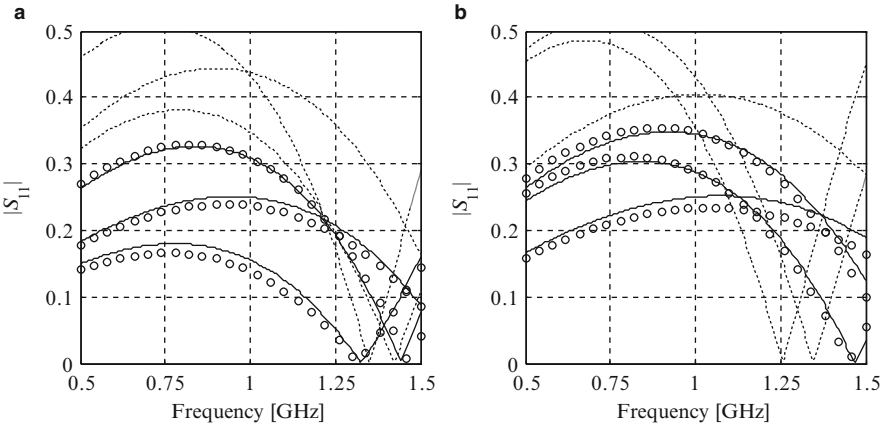

Fig. 20 NSM modeling of T-type SWRS components. Responses at the selected test designs—coarse model (*dotted line*), fine model (*solid line*), NSM surrogate after multipoint parameter extraction (*open circle*): (**a**) $\boldsymbol{R}_{s.cell}^{(1)}$; (**b**) $\boldsymbol{R}_{s.cell}^{(2)}$

The final design of compact RRC has been obtained after four iterations of the NSM algorithm. The footprint of the miniaturized structure is only $17 \times 27.3 = 464$ mm^2 and thus it offers a considerable miniaturization of almost 90 % with respect to the conventional circuit (4,536 mm^2).

The actual obtained −20 dB bandwidth is 23.5 %, which is broader than the one assumed in the specifications. The lower and upper operating frequencies are 0.915 and 1.150 GHz, respectively. A very slight shift of the operational frequency may be observed. What is also important, low-pass properties of SWRS components [73] introduced attenuation of harmonic frequencies up to 4 GHz. Narrow-band transmission characteristics of miniaturized RRC as well as a comparison of broadband responses of compact and conventional RRC is shown in Fig. 22.

A total design and optimization cost of the structure (∼8.6 h), including 11 $\boldsymbol{R}_{f.cell}^{(1)}$ and 11 $\boldsymbol{R}_{f.cell}^{(2)}$ model evaluations during generation of the inner space mapping layers, four $\boldsymbol{R}_f$ model simulations for RRC optimization, and evaluations of surrogate models ($\boldsymbol{R}_{s.g}$, $\boldsymbol{R}_{s.cell}^{(1)}$ and $\boldsymbol{R}_{s.cell}^{(2)}$) corresponds to about 1.2 simulations of $\boldsymbol{R}_f$ model. Additionally, the circuit has been optimized using alternative SBO techniques and direct optimization driven by pattern search algorithm. The NSM algorithm clearly outperforms the benchmark techniques. A detailed comparison of the methods in terms of iterations is provided in Table 3.

5 Conclusions

In this chapter, a technique for fast design and optimization of computationally expensive microwave/RF circuits with enhanced functionality has been discussed. The design procedure is based on a decomposition of conventional passive structure

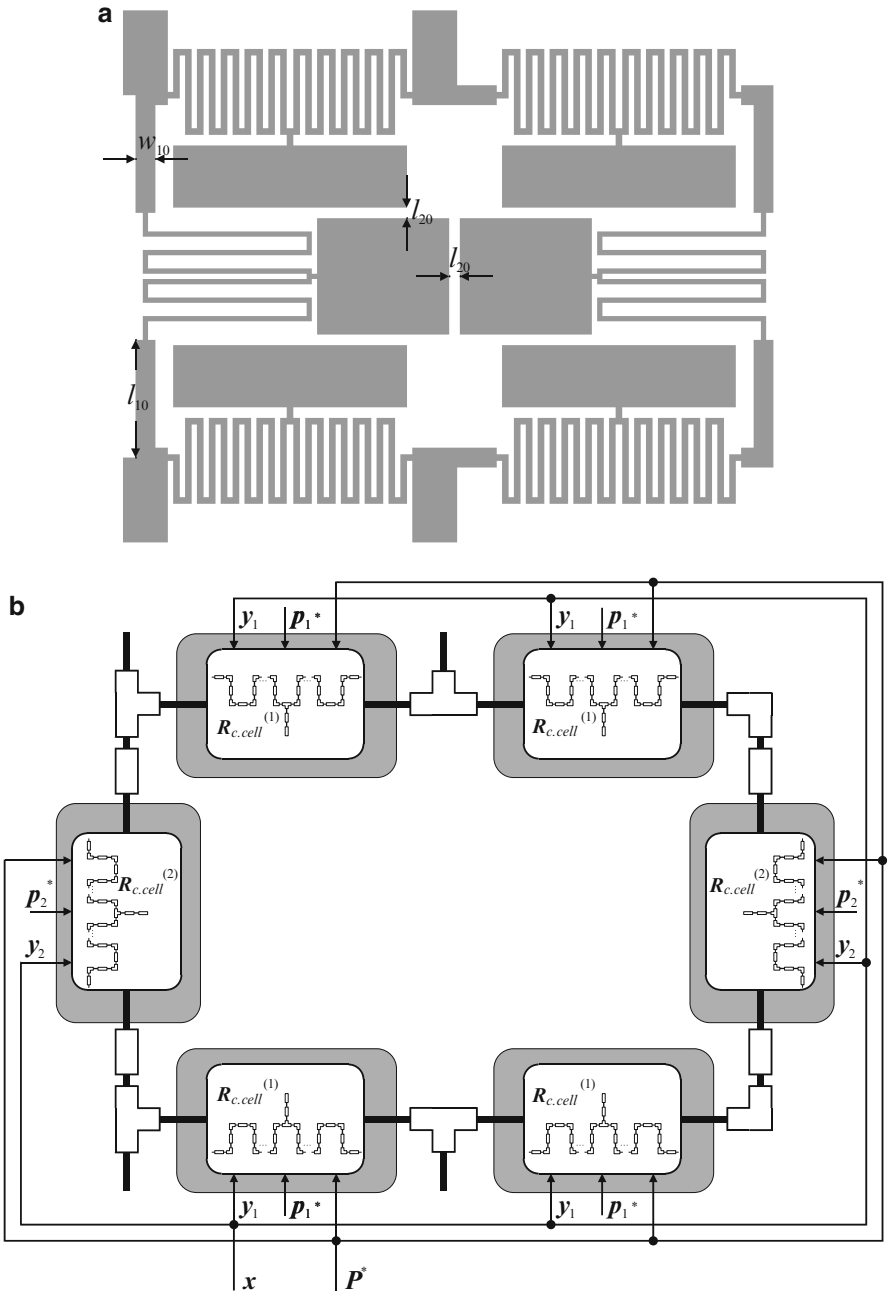

Fig. 21 A compact rat-race coupler composed of four $\boldsymbol{R}_{s.cell}{}^{(1)}$ and two $\boldsymbol{R}_{s.cell}{}^{(2)}$ T-type SWRS components: (**a**) geometry of an optimized structure; (**b**) schematic diagram of SWRS interconnections

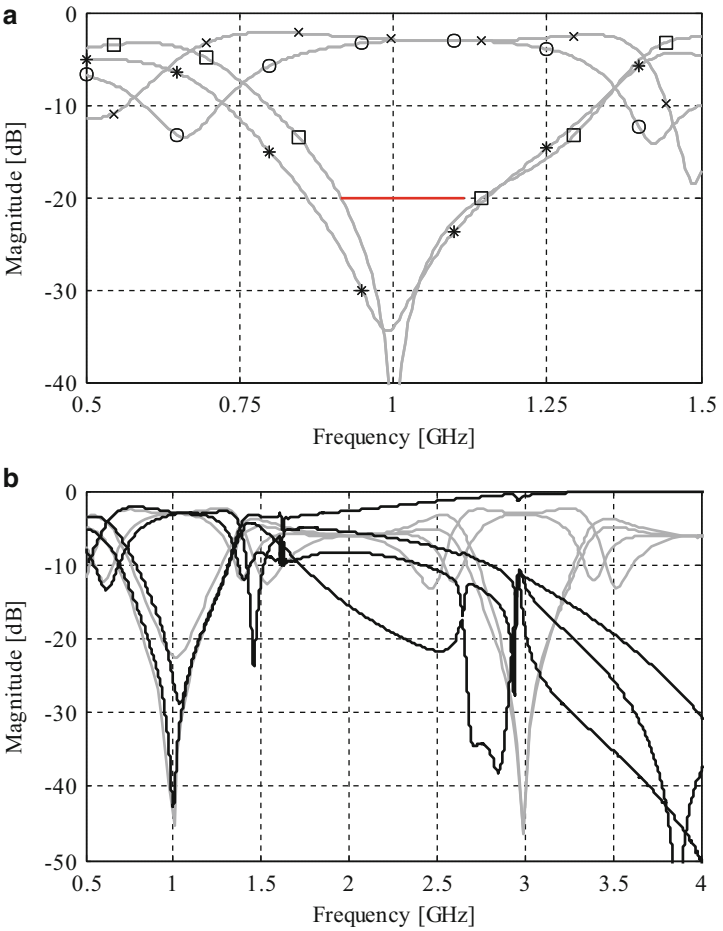

Fig. 22 A compact rat-race coupler: (**a**) transmission characteristics—(*asterisk*) reflection, (*open circle*) transmission, (*cross*) coupling, (*open square*) isolation; (**b**) attenuation of harmonic frequencies of compact RRC (*black line*) in comparison with conventional one (*gray line*)

Table 3 A compact rat-race coupler: design and optimization cost

	Optimization algorithm			
Model evaluations	NSM	ISM	SSM	Direct search
SWRS $\boldsymbol{R}_{s.cell}$	$0.9 \times \boldsymbol{R}_f$	N/A	N/A	N/A
SWRS $\boldsymbol{R}_{f.cell}$	$1.3 \times \boldsymbol{R}_f$	N/A	N/A	N/A
MT low-fidelity $\boldsymbol{R}_s$	$0.3 \times \boldsymbol{R}_f$	$3.9 \times \boldsymbol{R}_f$	$3.2 \times \boldsymbol{R}_f$	N/A
MT high-fidelity $\boldsymbol{R}_f$	4	16	12	286
Total cost	$6.5 \times \boldsymbol{R}_f$	$18.9 \times \boldsymbol{R}_f$	$15.2 \times \boldsymbol{R}_f$	$286 \times \boldsymbol{R}_f$
Total cost [h]	8.6	26.5	18.7	363.6

into a set of transmission line sections and their substitution with respective slow-wave resonant structures. Two distinct approaches for a determination of SWRS for transmission line replacement based on selection of a proper component from a predefined database and knowledge-based construction of the cell have been described.

Direct design of unconventional microwave/RF circuits constituted by SWRS components is a computationally expensive problem that may be efficiently handled only by means of surrogate-based optimization. Here, we discuss a NSM methodology, which is a two-stage design and optimization approach utilizing inner space mapping layer prepared at the level of each SWRS component, and the outer layer constructed at the level of the entire unconventional circuit. Representing of the design in such a way allows for a construction of a SWRS component model that exhibits good generalization capability and may be reused for the design various unconventional circuits.

The introduced technique allows for a fast and reliable design of computationally expensive circuits constituted of SWRS components. It is illustrated using three exemplary planar structures: a 16-variable four-section UWB matching transformer, a 15-variable three section broadband matching transformer, and a 10-variable rat-race coupler. All structures are successfully designed in a timeframe being only a fraction in comparison conventional design based on direct optimization scheme. Despite promising results, the discussed technique requires a considerable engineering knowledge to perform circuit decomposition and determine sufficient SWRS components. This is somehow problematic from the point of view of full automation of the design process. Expanding of the presented methods with the aim of design automation will be the subject of the future research.

References

1. Chen, S.-B., Jiao, Y.-C., Wang, W., Zhang, F.-S.: Modified T-shaped planar monopole antennas for multiband operation. IEEE Trans. Microw. Theory Tech. **54**, 3267–3270 (2006)
2. Xu, J., Miao, C., Cui, L., Ji, Y.-X., Wu, W.: Compact high isolation quad-band bandpass filter using quad-mode resonator. Electron. Lett. **48**, 28–30 (2012)
3. Liu, H.-W., Wang, Y., Wang, X.-M., Lei, J.-H., Xu, W.-Y., Zhao, Y.-L., Ren, B.-P., Guan, X.-H.: Compact and high selectivity tri-band bandpass filter using multimode stepped-impedance resonator. IEEE Microw. Wirel. Compon. Lett. **23**, 536–538 (2013)
4. Rodenbeck, C.T., Sang-Gyu, K., Wen-Hua, T., Coutant, M.R., Seungpyo, H., Mingyi, L., Kai, C.: Ultra-wideband low-cost phased-array radars. IEEE Trans. Microw. Theory Tech. **53**, 3697–3703 (2005)
5. Kuo, T.-N., Lin, S.-C., Chen, C.H.: Compact ultra-wideband bandpass filters using composite microstrip-coplanar-waveguide structure. IEEE Trans. Microw. Theory Tech. **54**, 3772–3778 (2006)
6. An-Shyi, L., Huang, T.-Y., Wu, R.-B.: A dual wideband filter design using frequency mapping and stepped-impedance resonators. IEEE Trans. Microw. Theory Tech. **56**, 2921–2929 (2008)
7. Zhang, X.-Y., Xue, Q.: High-selectivity tunable bandpass filters with harmonic suppression. IEEE Trans. Microw. Theory Tech. **58**, 964–969 (2010)

8. Sun, S., Zhu, L.: Periodically nonuniform coupled microstrip-line filters with harmonic suppression using transmission zero reallocation. IEEE Trans. Microw. Theory Tech. **53**, 1817–1822 (2005)
9. Ngoc-Anh, N., Ahmad, R., Yun-Taek, I., Yong-Sun, S., Seong-Ook, P.: A T-shaped wide-slot harmonic suppression antenna. IEEE Antennas Wirel. Propag. Lett. **6**, 647–650 (2007)
10. Deng, C., Li, P., Cao, W.: A high-isolation dual-polarization patch antenna with omnidirectional radiation patterns. IEEE Antennas Wirel. Propag. Lett. **11**, 1273–1276 (2012)
11. Zeng, S.-J., Wu, J.-Y., Tu, W.-H.: Compact and high-isolation quadruplexer using distributed coupling technique. IEEE Microw. Wirel. Compon. Lett. **21**, 197–199 (2011)
12. Chappell, W.J., Little, M.P., Katehi, L.P.B.: High isolation, planar filters using EBG substrates. IEEE Microw. Wirel. Compon. Lett. **11**, 246–248 (2001)
13. Hee-Ran, A., Itoh, T.: New isolation circuits of compact impedance-transforming 3-dB baluns for theoretically perfect isolation and matching. IEEE Trans. Microw. Theory Tech. **58**, 3892–3902 (2010)
14. Hee-Ran, A., Sangwook, N.: Compact microstrip 3-dB coupled-line ring and branch-line hybrids with new symmetric equivalent circuits. IEEE Trans. Micro. Theory Tech. **61**, 1067–1078 (2013)
15. Tao, Y., Pei-Ling, C., Itoh, T.: Compact quarter-wave resonator and its applications to miniaturized diplexer and triplexer. IEEE Trans. Microw. Theory Tech. **59**, 260–269 (2011)
16. Milligan, T.A.: Modern Antenna Design, 2nd edn. Wiley, New York (2005)
17. Pozar, D.M.: Microwave Engineering, 4th edn. Wiley, New York (2012)
18. Azadegan, R., Sarabandi, K.: Bandwidth enhancement of miniaturized slot antennas using folded, complementary, and self-complementary realizations. IEEE Trans. Antennas Propag. **55**, 2435–2444 (2007)
19. Ruiz-Cruz, J.A., Yunchi, Z., Zaki, K.A., Piloto, A.J., Tallo, J.: Ultra-wideband LTCC ridge waveguide filters. IEEE Microw. Wirel. Compon. Lett. **17**, 115–117 (2007)
20. Hou, J.-A., Wang, Y.-H.: Design of compact 90° and 180° couplers with harmonic suppression using lumped-element bandstop resonators. IEEE Trans. Microw. Theory Tech. **58**, 2932–2939 (2010)
21. Chen, W.-L., Wang, G.-M.: Exact design of novel miniaturised fractal-shaped branch-line couplers using phase-equalising method. IET Microw. Antennas Propag. **2**, 773–780 (2008)
22. Kaymaram, F., Shafai, L.: Enhancement of microstrip antenna directivity using double-superstrate configurations. Can. J. Electr. Comput. Eng. **32**, 77–82 (2007)
23. Opozda, S., Kurgan, P., Kitlinski, M.: A compact seven-section rat-race hybrid coupler incorporating PBG cells. Microw. Opt. Technol. Lett. **51**, 2910–2913 (2009)
24. Kurgan, P., Kitlinski, M.: Novel doubly perforated broadband microstrip branch-line couplers. Microw. Opt. Technol. Lett. **51**, 2149–2152 (2009)
25. Tseng, C.-H., Chen, H.-J.: Compact rat-race coupler using shunt-stub-based artificial transmission lines. IEEE Microw. Wirel. Compon. Lett. **18**, 734–736 (2008)
26. Kurgan, P., Bekasiewicz, A., Pietras, M., Kitlinski, M.: Novel topology of compact coplanar waveguide resonant cell low-pass filter. Microw. Opt. Technol. Lett. **54**, 732–735 (2012)
27. Bekasiewicz, A., Kurgan, P., Kitlinski, M.: A new approach to a fast and accurate design of microwave circuits with complex topologies. IET Microw. Antennas Propag. **6**, 1616–1622 (2012)
28. Nocedal, J., Wright, S.: Numerical Optimization, 2nd edn. Springer, New York (2006)
29. Rios, L.M., Sahinidis, N.V.: Derivative-free optimization: a review of algorithms and comparison of software implementations. J. Glob. Optim. **56**, 1247–1293 (2013)
30. Bakr, M.H., Nikolova, N.K.: An adjoint variable method for time domain TLM with wideband Johns matrix boundaries. IEEE Trans. Microw. Theory Tech. **52**, 678–685 (2004)
31. Chung, Y.S., Cheon, C., Park, I.H., Hahn, S.Y.: Optimal design method for microwave device using time domain method and design sensitivity analysis-part II: FDTD case. IEEE Trans. Magn. **37**, 3255–3259 (2001)
32. El Sabbagh, M.A., Bakr, M.H., Bandler, J.W.: Adjoint higher order sensitivities for fast full-wave optimization of microwave filters. IEEE Trans. Microw. Theory Tech. **54**, 3339–3351 (2006)

33. Koziel, S., Mosler, F., Reitzinger, S., Thoma, P.: Robust microwave design optimization using adjoint sensitivity and trust regions. Int. J. RF Microw. Comput. Aid. Eng. **22**, 10–19 (2012)
34. Deb, K.: Multi-Objective Optimization Using Evolutionary Algorithms. Wiley, Chichester (2001)
35. Talbi, E.-G.: Metaheuristics – From Design to Implementation. Wiley, Chichester (2009)
36. Bandler, J.W., Cheng, Q.S., Dakroury, S.A., Mohamed, A.S., Bakr, M.H., Madsen, K., Søndergaard, J.: Space mapping: the state of the art. IEEE Trans. Microw. Theory Tech. **52**, 337–361 (2004)
37. Echeverría, D., Hemker, P.W.: Manifold mapping: a two-level optimization technique. Comput. Vis. Sci. **11**, 193–206 (2008)
38. Koziel, S., Leifsson, L., Ogurtsov, S.: Reliable EM-driven microwave design optimization using manifold mapping and adjoint sensitivity. Microw. Opt. Technol. Lett. **55**, 809–813 (2013)
39. Koziel, S.: Shape-preserving response prediction for microwave design optimization. IEEE Trans. Microw. Theory Tech. **58**, 2829–2837 (2010)
40. Leifsson, L., Koziel, S.: Multi-fidelity design optimization of transonic airfoils using physics-based surrogate modeling and shape-preserving response prediction. J. Comput. Sci. **1**, 98–106 (2010)
41. Koziel, S., Cheng, Q.S., Bandler, J.W.: Space mapping. IEEE Microw. Magazine **9**, 105–122 (2008)
42. Koziel, S., Bandler, J.W., Madsen, K.: A space mapping framework for engineering optimization: theory and implementation. IEEE Trans. Microw. Theory Tech. **54**, 3721–3730 (2006)
43. Koziel, S., Bekasiewicz, A., Zieniutycz, W.: Expedited EM-driven multi-objective antenna design in highly-dimensional parameter spaces. IEEE Antennas Wirel. Propag. Lett. **13**, 631–634 (2014)
44. Redhe, M., Nilsson, L.: Optimization of the new Saab 9-3 exposed to impact load using a space mapping technique. Struct. Multidiscip. Optim. **27**, 411–420 (2004)
45. Crevecoeur, G., Dupre, L., Van de Walle, R.: Space mapping optimization of the magnetic circuit of electrical machines including local material degradation. IEEE Trans. Magn. **43**, 2609–2611 (2007)
46. Encica, L., Makarovic, J., Lomonova, E.A., Vandenput, A.J.A.: Space mapping optimization of a cylindrical voice coil actuator. IEEE Trans. Ind. Appl. **42**, 1437–1444 (2006)
47. Bandler, J.W., Cheng, Q.S., Nikolova, N.K., Ismail, M.A.: Implicit space mapping optimization exploiting preassigned parameters. IEEE Trans. Microw. Theory Tech. **52**, 378–385 (2004)
48. Cheng, Q.S., Bandler, J.W., Koziel, S.: Combining coarse and fine models for optimal design. IEEE Microw. Magazine **9**, 79–88 (2008)
49. Koziel, S., Bandler, J.W., Cheng, Q.S.: Constrained parameter extraction for microwave design optimisation using implicit space mapping. IET Microw. Antennas Propag. **5**, 1156–1163 (2011)
50. Kurgan, P., Bekasiewicz, A.: A robust design of a numerically demanding compact rat-race coupler. Microw. Opt. Technol. Lett. **56**, 1259–1263 (2014)
51. Koziel, S., Bekasiewicz, A., Kurgan, P.: Rapid EM-driven design of compact RF circuits by means of nested space mapping. IEEE Microw. Wirel. Compon. Lett. **24**(6), 364–366 (2014)
52. Awida, M.A., Safwat, A.M.E., El-Hennawy, H.: Compact rat-race hybrid coupler using meander space-filling curves. Microw. Opt. Technol. Lett. **48**, 606–609 (2006)
53. Eccleston, K.W., Ong, S.H.M.: Compact planar microstrip line branch-line and rat-race couplers. IEEE Trans. Microw. Theory Tech. **51**, 2119–2125 (2003)
54. Kurgan, P., Kitlinski, M.: Doubly miniaturized rat-race hybrid coupler. Microw. Opt. Technol. Lett. **53**, 1242–1244 (2011)
55. Kurgan, P., Kitlinski, M.: Novel microstrip low-pass filters with fractal defected ground structures. Microw. Opt. Technol. Lett. **51**, 2473–2477 (2009)
56. Wen, W., Lu, Y., Fu, J.S., Yong, Z.X.: Particle swarm optimization and finite-element based approach for microwave filter design. IEEE Trans. Magnetics **41**, 1800–1803 (2005)

57. Lai, M.-I., Jeng, S.-K.: Compact microstrip dual-band bandpass filters design using genetic-algorithm techniques. IEEE Trans. Microw. Theory Tech. **54**, 160–168 (2006)
58. Chen, C.-F., Lin, C.-Y., Weng, J.-H., Tsai, K.-L.: Compact microstrip broadband filter using multimode stub-loaded resonator. Electron. Lett. **49**, 545–546 (2013)
59. Meissner, P., Kitlinski, M.: A 3-dB multilayer coupler with UC-PBG structure. IEEE Microw. Wirel. Compon. Lett. **15**, 52–54 (2005)
60. Lin, B.-Q., Zheng, Q.-R., Yuan, N.-C.: A novel planar PBG structure for size reduction. IEEE Microw. Wirel. Compon. Lett. **16**, 269–271 (2006)
61. Hong, J.-S., Lancaster, M.J.: Theory and experiment of novel microstrip slow-wave open-loop resonator filters. IEEE Trans. Microw. Theory Tech. **45**, 2358–2365 (1997)
62. García-García, J., Bonache, J., Gil, I., Martín, F., Marqués, R., Falcone, F., Lopetegi, T., Laso, M.A.G., Sorolla, M.: Comparison of electromagnetic band gap and split-ring resonator microstrip lines as stop band structures. Microw. Opt. Technol. Lett. **44**, 376–379 (2005)
63. Zhang, F.: High-performance rat-race hybrid ring for RF communication using MEBE-on-microstrip technology. Microw. Opt. Technol. Lett. **51**, 1539–1542 (2009)
64. Nanbo, J., Rahmat-Samii, Y.: Hybrid real-binary particle swarm optimization (HPSO) in engineering electromagnetics. IEEE Trans. Antennas Propag. **58**, 3786–3794 (2010)
65. Lai, M.-I., Jeng, S.-K.: A microstrip three-port and four-channel multiplexer for WLAN and UWB coexistence. IEEE Trans. Microw. Theory Tech. **53**, 3244–3250 (2005)
66. Nishino, T., Itoh, T.: Evolutionary generation of microwave line-segment circuits by genetic algorithms. IEEE Trans. Microw. Theory Tech. **50**, 2048–2055 (2002)
67. Smierzchalski, M., Kurgan, P., Kitlinski, M.: Improved selectivity compact band-stop filter with Gosper fractal-shaped defected ground structures. Microw. Opt. Technol. Lett. **52**(1), 227–232 (2010)
68. Zhang, C.F.: Planar rat-race coupler with microstrip electromagnetic bandgap element. Microw. Opt. Technol. Lett. **53**, 2619–2622 (2011)
69. Bekasiewicz, A., Kurgan, P.: A compact microstrip rat-race coupler constituted by nonuniform transmission lines. Microw. Opt. Technol. Lett. **56**, 970–974 (2014)
70. Matthaei, G., Jones, E.M.T., Young, L.: Microwave Filters, Impedance-Matching Networks, and Coupling Structures. Artech House, Norwood (1980)
71. Hong, J.-S., Lancaster, M.J.: Microstrip Filters for RF/Microwave Applications. Wiley, Hoboken (2001)
72. Kurgan, P., Kitlinski, M.: Slow-wave fractal-shaped compact microstrip resonant cell. Microw. Opt. Technol. Lett. **52**, 2613–2615 (2010)
73. Kurgan, P., Filipcewicz, J., Kitlinski, M.: Development of a compact microstrip resonant cell aimed at efficient microwave component size reduction. IET Microw. Antennas Propag. **6**, 1291–1298 (2012)
74. Kurgan, P., Filipcewicz, J., Kitlinski, M.: Design considerations for compact microstrip resonant cells dedicated to efficient branch-line miniaturization. Microw. Opt. Technol. Lett. **54**, 1949–1954 (2012)
75. Bekasiewicz, A., Koziel, S.: Local–global space mapping for rapid EM-driven design of compact RF structures. Int. Conf. Microw. Radar Wirel. Commun. **1**, 313–316 (2014)
76. Koziel, S., Kurgan, P.: Low-cost optimization of compact branch-line couplers and its application to miniaturized Butler matrix design. Eur. Microw. Conf. Rome, Italy, Oct. 5–10, (2014)
77. Koziel, S., Echeverría-Ciaurri, D., Leifsson, L.: Simulation-driven design in microwave engineering: methods. In: Koziel, S., Yang, X.S. (eds.) Computational Optimization, Methods and Algorithms. Series: Studies in Computational Intelligence, pp. 33–60. Springer, New York (2011)
78. Cheng, Q.S., Rautio, J.C., Bandler, J.W., Koziel, S.: Progress in simulator-based tuning—the art of tuning space mapping [application notes]. IEEE Microw. Magazine **11**, 96–110 (2010)
79. Bandler, J.W., Cheng, Q.S., Hailu, D.M., Nikolova, N.K.: A space-mapping design framework. IEEE Trans. Microw. Theory Tech. **52**, 2601–2610 (2004)

80. Kolda, T.G., Lewis, R.M., Torczon, V.: Optimization by direct search: new perspectives on some classical and modern methods. SIAM Rev. **45**, 385–482 (2003)
81. Goldberg, D.E.: Genetic Algorithms in Search, Optimization and Machine Learning. Addison-Wesley, New York (1989)
82. Koziel, S., Echeverría-Ciaurri, D., Leifsson, L.: Surrogate-based methods. In: Koziel, S. Yang, X.S. (eds.) Computational Optimization, Methods and Algorithms. Series: Studies in Computational Intelligence, pp. 33–60. Springer, New York (2011)
83. Koziel, S., Leifsson, L., Ogurtsov, S.: Space mapping for electromagnetic-simulation-driven design optimization. In: Koziel, S. Leifsson, L. (eds.) Surrogate-Based Modeling and Optimization: Applications in Engineering, pp. 1–25. Springer, New York (2013)
84. CST Microwave Studio, ver. 2013.: CST AG, Bad Nauheimer Str. 19, D-64289 Darmstadt, Germany (2013)
85. Agilent ADS, ver. 2011.10: Agilent Technologies, 1400 Fountaingrove Parkway, Santa Rosa, CA 95403-1799, (2011)